American Mineralogist, Volume 83, pages 458–475, 1998

Fe-Mg order-disorder in tremolite–actinolite–ferro-actinolite at ambient and high temperature

BERNARD W. EVANS[1] AND HEXIONG YANG[2]

[1]Department of Geological Sciences, Box 351310, University of Washington, Seattle, Washington 98195-1310, U.S.A.
[2]Geophysical Laboratory, 5251 Broad Branch Road, NW, Washington, D.C. 20015-1305, U.S.A.

ABSTRACT

The crystal structures and M-site populations of a series of unheated and heat-treated, near-binary members of the actinolite series were determined from single-crystal X-ray diffraction data. Small, systematic differences in crystal structure (mean and individual bond lengths, octahedral distortions, and Mg-Fe site preferences) between the actinolite and cummingtonite series are documented and rationalized in terms of the bond-valence model. Mg-Fe^{2+} site preferences among the M1, M2, and M3 sites in the actinolite series are small. Between M1 and M3, site preference (Fe^{2+} slightly in favor of M1) is independent of temperature. Mg is favored in M2 over M1 in unheated samples (less strongly than in cummingtonite-grunerite), but Fe^{2+} and Mg are virtually disordered in samples re-equilibrated at 700 °C. Site preference between M2 and M3 and possibly also between M1 and M2 appears to undergo a reversal as a result of heat treatment, but consideration of all sources of error renders this conclusion a tentative one, although the observation could be explained in terms of a bond valence deficiency. The ratio of Fe^{2+}/Mg atoms on M4 cannot be accurately determined, but refinements indicate that, like cummingtonite-grunerite, it is larger than on all other M sites. Expansion of the cell dimensions with an increase in Fe/Mg ratio follows a pattern similar to that of thermal expansion, and a and β are influenced by cummingtonite-grunerite solid solution. The data are consistent with a cell volume of 942.8 $Å^3$ (or molar volume of 2.8388 J/bar) for end-member ferro-actinolite, a first approximation that assumes a reciprocal, quadrilateral ΔV of zero.

INTRODUCTION

Successful thermodynamic modeling of the solution properties of multisite minerals such as the amphiboles requires a description of the temperature, pressure, and compositional dependence of atom ordering on sites. This information is needed to make an informed decision on the degree of complexity of the solution model that is ultimately adopted. Ordering of Mg and Fe^{2+} on the M cation sites of amphiboles is known to proceed down to temperatures as low as ~300 °C, and amphiboles in numerous terrestrial parageneses are participants in equilibria corresponding to temperatures at which site fractionation is pronounced. Configurational entropies may be calculated directly from such data, and the overall energetics of solution (enthalpy and Gibbs energy) show a temperature and composition dependency that reflects the ordering states (e.g., Ghiorso et al. 1995).

An earlier study (Hirschmann et al. 1994) presented the results of a single-crystal X-ray diffraction study (XRD) of heat-treated and quenched natural amphiboles on the cummingtonite–grunerite binary join. This companion study of the upper join in the Ca-Mg-Fe amphibole quadrilateral, tremolite–actinolite–ferro-actinolite (the actinolite series, for short), was conducted to complete a database of ordering and crystallographic information for the series, which will assist calculation of the thermodynamic solution properties of the entire amphibole quadrilateral. The only possibility for order-disorder in strictly quadrilateral amphiboles, of course, is Fe^{2+} and Mg on the M sites.

The actinolite series, ideally $\square Ca_2(Mg,Fe)_5Si_8O_{22}(OH)_2$, has a crystal structure characterized by double silicate chains running parallel to c. The chains are composed of two crystallographically distinct tetrahedra, T1 and T2, and are linked together by strips of cations occupying three nonequivalent octahedra, M1, M2, and M3, and an eightfold-coordinated polyhedron, M4. Published X-ray structure refinements of members of the actinolite series include very few that are significantly Fe-bearing and none whose state of order has been re-equilibrated at high temperature. Refinement of a natural manganoan ferro-actinolite (Mitchell et al. 1970, 1971) showed nearly random mixing of Fe^{2+} and Mg on the octahedral sites M1, M2, and M3: $Fe^{2+}/(Fe^{2+}+Mg)$ = 0.61(M1), 0.57(M2), and 0.58(M3); in this refinement all Mn, and no Fe, was assigned to M4, and Fe^{3+} was assigned to M2. A low-Fe actinolite was refined by Litvin et al. (1972) and Litvin (1973). If in this sample Fe^{3+} is assigned to M2 (Hawthorne 1983, p. 382) rather than equally to M1, M2, and M3, then there is a preference of Mg for M2 and Fe^{2+}

0003–004X/98/0506–0458$05.00

TABLE 1. Sample characteristics

Specimen no.	Rock type	Fe/(Fe + Mg) (%)	Location	References
NMNH 93728	act-talc rock	11–12	Greiner, Zillertal, Austria	(1)
67-3172	cpx hornfels	18–19	Carr Fork Mine, Bingham, Utah	(2)
67-3701	cpx hornfels	23	Carr Fork Mine, Bingham, Utah	(2)
NMNH 156831	uralite from cpx	27–38	Green Monster Mine, Prince of Wales Is., Alaska	(3)
11B	iron formation	53–54	Luce Lake, Labrador, Canada	(4), (5), (6)
12BA	iron formation	53	Bloom Lake, Quebec, Canada	(5), (6), (7)
AMNH 44973	quartzite	57–59	Cumberland, Rhode Island	(6), (8), (9)
ID4-4C	iron formation	62	Isua Belt, East Greenland	(10)
NMNH 168215	alteration of hbl	81–85	Goose Creek Quarry, Leesburg, Virginia	

Notes: (1) Skogby and Annersten (1985; cf. sample 679), (2) Atkinson and Einaudi (1978), (3) Kennedy (1953), (4) Klein (1966), (5) Wilkins (1970), (6) Burns and Greaves (1971), (7) Mueller (1960), (8) Mustard (1992), (9) Mitchell et al. (1970, 1971), (10) Dymek and Klein (1988).

for M1 and M3; however, the cummingtonite component (21%) reported in this actinolite is suspiciously large. These actinolite site-occupancies are similar to those in the cummingtonite series, except that the preference of Mg for M2 appears to be less strong in the actinolites. Measurements using infrared and Mössbauer absorption spectroscopy, notwithstanding ongoing reassessments (Wilkins 1970; Burns and Greaves 1971; Goldman and Rossman 1977; Goldman 1979), have suggested stronger site preferences for Fe and Mg atoms between the M1 + M3 and M2 sites than the X-ray refinements. In all these studies, no Mg was placed on M4.

Synthetic and natural tremolites and actinolites (up to 13% ferro-actinolite end-member) were studied by Mössbauer spectroscopy at 77 K following heat treatment at 600 to 800 °C by Skogby and Annersten (1985), Skogby (1987), and Skogby and Ferrow (1989). Fe^{2+} was found to strongly favor M4 over M2 and slightly favor M1 + M3 over M2. A decrease in equilibration temperature was accompanied by the transfer of some Fe^{2+} from M2 to M4, while the contents of M1 + M3 were unchanged.

Many more X-ray structure refinements have been done on aluminous calcic amphiboles or hornblende sensu lato. Relative to Mg, the Fe^{2+} preference on the M-sites is M3>M1>M2 (Robinson et al. 1973; Litvin 1973; Hawthorne and Grundy 1973, 1977, 1978; Bocchio et al. 1978; Hawthorne et al. 1980; Ungaretti et al. 1983; Phillips et al. 1988; Makino and Tomita 1989; Oberti et al. 1993a, 1995a, 1995b). The preference of Fe^{2+} for M3 over M1 is consistent although not strong, differing significantly from quadrilateral amphiboles. The reported ratio of Fe^{2+}/Mg of M2 is variable; its accuracy suffers from the difficulty of assessing the content of other cations occupying that site, such as Al, Fe^{3+}, Ti, and Cr. It has been claimed that high-temperature (volcanic) hornblendes have Fe^{2+} and Mg randomly distributed on M1, M2, and M3, in contrast to low-temperature (metamorphic and skarn) samples (Makino and Tomita 1989). There are no published accounts of X-ray diffraction studies of temperature-dependent M-site ordering in hornblendes based on heat treatment.

We report the results of single-crystal X-ray structure refinements of unheated and heat-treated natural samples of the actinolite series covering a range of macroscopic $Fe^{2+}/(Fe^{2+}+Mg)$ values from 10 to 85%. Natural rather than synthetic actinolites were chosen because their relative freedom from crystal defects (e.g., Ahn et al. 1991; Maresch et al. 1994), their larger crystal size, and their ease of characterization offset slight departures from binary compositions. Given the decreased resolution of Mössbauer spectra of actinolite with increasing Fe content (Goldman 1979; Skogby and Annersten 1985) and the site resolution of XRD, we chose the latter as the preferred technique to determine the M-site occupancies of actinolite as a function of temperature. We discovered that the M1, M2, and M3 site preferences in the actinolite series as a whole are not pronounced, and therefore concentrated primarily on a comparison between unheated samples and samples re-equilibrated hydrothermally and under reducing conditions at high temperature, mostly 700 °C.

EXPERIMENTAL PROCEDURES

Specimen preparation

Electron microprobe analysis (see below) was used to select samples of naturally occurring members of the actinolite series (Table 1) from an extensive collection assembled from many sources (see Acknowledgments) by rejecting those with more than minimal amounts of non-quadrilateral components. To obtain a wide spread in bulk X_{Fe} contents, this meant including some samples with variable Fe/Mg ratios from grain to grain (e.g., sample NMNH 156831). Fe-rich actinolites with very small Al, Na, and Fe^{3+} contents are quite rare. The best source rocks were found to be metamorphosed banded iron formations and skarns where calcic pyroxene had been replaced by uralitic actinolite. Almost all samples show minor correlated variations in Na, Al, Si, Mg, and Fe, representing incipient coupled substitutions of the types that lead to hornblende. The final list (Table 1) comprises near-binary actinolites with <1 to 10% cummingtonite in solution. Samples were crushed, washed, sieved, and purified with a Frantz magnetic separator, when necessary also with heavy liquids, and by final hand-picking.

Heat treatment was performed by sealing 20–80 mg of the sample with 5–10 mg distilled H_2O in annealed $Ag_{60}Pd_{40}$ capsules 2–3 cm long, enclosing three at a time

TABLE 2. Percent ferrous iron/total iron in actinolite series samples

Specimen no.	Run no.	*T* (°C)	WC	PM	MS	XREF	Preferred value
NMNH 93728	unheated			79.4/83.1	90	89	86
NMNH 93728	C78	700		89.6		100	94
67-3172	unheated			81.3		86	84
67-3172	C70	700		90.6		89	90
67-3701	unheated			74.7		86	84
67-3701	C71	700		88.9		90	90
NMNH 156831	unheated			86.7	98	94.5	91
NMNH 156831	C79	700		*		98	94
11B	unheated		100(1)	95.8/94.2	96	95	95
11B	C46	600		98.7		95	96
11B	C28	700		94.7		94	96
11B	C41	800		96.8		93	96
12BA	unheated		92.2(2)	91.3		93	93
12BA	C60	700		97.7		95	96
AMNH 44973	unheated		88.7(3)	86.6/91.1		90	90
AMNH 44973	C59	700		95.6		94	94
ID4-4C	unheated			97.3		95	96
ID4-4C	C51	700		97.5		95	96
NMNH 168215	unheated			88.3		98	97
NMNH 168215	C80	700				98	97

Notes: Percents as determined previously by wet chemistry (WC), by photochemical methods at University of Illinois (PM), by Mössbauer spectroscopy (MS), and from mean bond length ⟨M2-O⟩ (XREF). WC literature data: (1) Klein (1966, Table 5), J. Ito analysis; (2) Burns and Greaves (1971, Table 1), J.H. Scoon analysis, sample from Mueller (1960); (3) Mitchell et al. (1970), P. Elmore and E. Little, analysis; see also Burns and Greaves (1971).
* Lost in mail.

with steel and carbon filler rods in cold-seal pressure vessels, and raising the vessels to two kbar of CH_4 pressure. With one exception (experiment C51, 24 h), experiment duration was between 48 and 71 h at 700 °C, 31 d at 600 °C, and 4 h at 800 °C. Skogby (1987) showed that equilibrium disorder in tremolite was reached in 5 d at 650 °C or in 5 h at 750 °C. The temperature of treatment is believed accurate to within ± 10 °C. Vessels were quenched inside a coil of air jets, which achieved a cooling rate of 7 °C per s over the first 200 °C of cooling. The reducing atmosphere inside the pressure vessels in some cases caused a reduction in the green color of the sample powder and in most of them a measurable increase in ratio Fe^{2+}/Fe_{total} (Table 2).

X-ray diffraction

A single crystal was selected from each sample and checked for crystal quality using ω-scans of diffraction peak shapes. Some of the unit-cell dimensions and X-ray diffraction intensities of suitable crystals were measured at the University of Washington, Seattle, on a four-circle diffractometer (Huber 512) equipped with a graphite monochromator using Mo*K*α radiation (50 kV and 32 mA); the remainder (Table 3) were measured on a Sie-

TABLE 3. Crystal data and refinement statistics for actinolite series samples

Specimen no.	*a* (Å)	*b* (Å)	*c* (Å)	β (°)	*V* (Å³)	Total reflections.	Reflections. $>3\sigma_I$	R_w	*R*	Note
NMNH 93728	9.834(1)	18.078(2)	5.283(1)	104.63(1)	908.8	1771	1318	0.039	0.037	CU
C78	9.833(1)	18.078(2)	5.282(1)	104.58(1)	908.7	1830	1417	0.043	0.036	CU
67-3172	9.855(1)	18.069(3)	5.283(1)	104.79(1)	909.6	1835	1378	0.038	0.031	UW
C70	9.852(1)	18.066(2)	5.282(1)	104.89(1)	908.6	1845	1483	0.033	0.026	UW
67-3701	9.866(2)	18.098(4)	5.284(1)	104.77(1)	912.3	1780	1042	0.037	0.043	CU
C71	9.863(2)	18.090(4)	5.282(1)	104.78(1)	911.2	1857	1459	0.040	0.031	UW
NMNH 156831	9.881(1)	18.139(2)	5.298(1)	104.78(1)	918.1	1777	1287	0.041	0.036	UW
C79	9.886(1)	18.150(2)	5.300(1)	104.79(1)	919.5	1791	1174	0.043	0.044	CU
11B	9.891(1)	18.190(2)	5.297(1)	104.54(1)	922.5	1793	1413	0.043	0.036	CU
C46	9.890(1)	18.198(2)	5.296(1)	104.57(1)	922.5	1870	1543	0.036	0.028	UW
C28	9.891(1)	18.200(1)	5.296(1)	104.55(1)	922.8	1872	1568	0.039	0.031	UW
C41	9.890(1)	18.192(2)	5.294(1)	104.53(1)	922.0	1859	1643	0.037	0.027	UW
12BA	9.886(1)	18.171(2)	5.297(1)	104.61(1)	920.7	1876	1261	0.043	0.035	UW
C60	9.900(1)	18.198(1)	5.299(1)	104.63(1)	923.7	1872	1427	0.035	0.027	UW
AMNH 44973	9.884(1)	18.189(2)	5.302(1)	104.60(1)	922.4	1855	1400	0.044	0.033	UW
C59	9.890(2)	18.194(3)	5.306(1)	104.62(1)	923.8	1865	1497	0.037	0.027	UW
ID4-4C	9.908(2)	18.218(3)	5.301(1)	104.59(1)	926.0	1801	1141	0.038	0.040	CU
C51	9.903(1)	18.211(2)	5.299(1)	104.64(1)	924.6	1884	1520	0.038	0.030	UW
NMNH 168215	9.977(2)	18.287(3)	5.308(1)	104.81(1)	936.3	1814	1191	0.036	0.035	CU
C80	9.986(2)	18.296(4)	5.306(1)	104.79(1)	937.3	1820	1299	0.051	0.047	CU

Note: CU = University of Colorado at Boulder; UW = University of Washington at Seattle.

mens P4 four-circle diffractometer at the University of Colorado, Boulder. All unit-cell dimensions were determined by least-squares refinements of 20 to 30 reflections with $20° < 2\theta < 35°$. XRD intensity data of one quadrant of reciprocal space up to $2\theta = 65°$ were collected in the ω-scan mode at a scan speed of 3° per minute at the University of Washington, and with a constant-precision θ–2θ scan mode with variable speed scans at the University of Colorado. Three standard reflections were checked after every 97 reflections; no systematic or significant variation in the intensities of the standard reflections was observed. All X-ray intensity data were corrected for Lorentz and polarization effects. A semi-empirical absorption correction method (North et al. 1968) was applied to the data collected at the University of Washington, and an analytical method to the data collected at the University of Colorado. Only reflections having intensities $\geq 3\sigma_I$ were considered as observed and included in the refinements, where σ_I is the standard deviation determined from the counting statistics.

Chemical analysis

The chemical compositions of the crystals used for the X-ray data measurements were determined by wavelength-dispersive analysis with a JEOL 733 microprobe at the University of Washington (Table 4). Our analytical procedure was the same as in the cummingtonite study by Hirschmann et al. (1994, p. 865). At least ten spots per crystal were measured and then averaged. Compositions were recast to formula proportions incorporating an independent estimate of Fe_2O_3 and variable formula bases as described below.

Ferrous iron and total iron were determined in sample powders by J. Wu and J.W. Stucki at the University of Illinois by a photochemical method that utilizes the same aliquot (Stucki and Anderson 1981; Stucki 1981; Komadel and Stucki 1988). The method is accurate to within 2–5% (J.W. Stucki, personal communication). An estimate of ferrous and ferric iron was also made (Table 2) from refined site occupancies of total Fe using the regression equation of Hawthorne (1983, Table 27) for the mean bond-length ⟨M2-O⟩ of *C*2/*m* amphiboles: $\langle M2\text{-}O\rangle = 1.488 + 0.827\langle r_{M2}\rangle$, (where $\langle r\rangle$ is the mean ionic radius) under the assumption of complete Fe^{3+} ordering on M2. The two methods for the percent of ferrous iron/total iron agree to within 3% for more than half our samples (Table 2). Larger differences may be attributed to one or more of the following: analytical error, poorer precision at lower total iron contents, and error in our assumption of complete ordering of Fe^{3+} on M2 (discussed below). Independent measures of redox state by wet-chemical analysis were available in the literature for three samples and by Mössbauer spectrometry for an additional three (Table 2). To compute formulae, we opted to use compromise ''preferred'' values of Fe^{2+}/total Fe (Table 2), realizing that they are not well established for some samples, and that this has implications for our estimates of Fe^{2+} on the octahedral sites.

With few exceptions, the photo-chemical and M2 bond-length data both show that the Fe^{3+} in our samples was partially reduced as a result of their heat treatment in H_2O-fluid buffered on CCH_4. This is especially true for two actinolites from skarns (67-3172 and 67-3701), which is not surprising because they are believed (Atkinson and Einaudi 1978) to have formed at an f_{O_2} corresponding to about HM-1 log unit (~NNO + 3). The ferro-actinolites from metamorphosed banded iron formations were poor in Fe^{3+} at the outset; ferro-actinolites 11B, 12BA, and ID4-4C coexisted with cummingtonite containing 64, 61, and 69% grunerite component, respectively, indicating that these rocks equilibrated under log f_{O_2} conditions less than NNO + 1 (Evans and Ghiorso 1995). The generally small amount of Fe^{3+} in naturally occurring actinolites, as compared to all calcic and subcalcic amphiboles, is well known (Leake 1968; Popp et al. 1995, in Fig. 1C).

The results of our heat treatments are consistent with published experimental studies, which have strongly suggested that the proportions of Fe^{3+} and Fe^{2+} in calcic amphibole can be re-equilibrated in response to newly imposed gas compositions in a few days at 600 °C or higher. For example, Skogby and Annersten (1985) showed that natural tremolites and Mg-rich actinolites could be reduced by heating in a hydrogen atmosphere for 7 h at 600 °C. Clowe et al. (1988) found that steady-state values of ferric/ferrous ratios in magnesio-hornblende and tschermakitic hornblende could be achieved in oxygen-buffered hydrothermal experiments at 650 °C and 1 kbar in experiments of 4 to 8 d duration. Popp et al. (1995) showed that equilibrium values of Fe^{3+}/Fe_{total} in kaersutite (0.12) could be attained in about 2 d at 700 °C and 1 kbar on the CCH_4 buffer. These authors attributed experimentally induced changes in ferrous/ferric ratio to progress in either direction of the dehydrogenation (oxy-amphibole) reaction: $Fe^{2+} + OH^- = Fe^{3+} + O^{2-} + \frac{1}{2}H_2$, and we agree with this inference. In our case, hydrothermal heat treatment at 700 °C on the CCH_4 buffer caused hydrogenation and partial reduction of Fe^{3+} to Fe^{2+}. However, not all the Fe^{3+} was reduced, even though this buffer is three log f_{O_2} units below NNO. Some of the remaining Fe^{3+} represents group C ferric iron that is charge-balanced against the cations ^{T}Al or ^{B}Na, substitutions that probably cannot readily be influenced by laboratory treatment. However, four of our ferro-actinolites (11B, 12BA, ID4-4C, NMNH 168215) are so low in Al and Na (Table 4) that cation-balanced substitutions cannot account for much of the Fe^{3+} remaining after heat treatment. These samples are sufficiently close to binary Fe-Mg solid solutions that formula constraints are indicative of the type of Fe^{3+} substitution. Given the analytical values of Fe^{3+}, satisfactory formulae (Si + Al ≥ 8.000, and Σcations except K ≥ 15.000) can only be obtained if analyses are recast on the assumption that some oxy-amphibole component is present, that is, having a formula basis with more than 23.0 anhydrous O atoms. (Without independent analysis of H, the relative proportions of cation-charge and anion-charge

TABLE 4. Chemical analyses of actinolite series crystals with formulae

Sample no.	93728	93728	67-3172	67-3172	67-3701	67-3701	156831	156831	11B
Treatment no.	–	C78	–	C70	–	C71	–	C79	–
SiO_2	57.73	57.50	55.57	55.54	55.10	55.04	54.84	52.65	53.52
TiO_2	0.02	0.00	0.13	0.04	0.09	0.05	0.01	0.12	0.00
Al_2O_3	0.75	0.85	1.53	1.20	1.53	1.06	1.16	2.48	0.05
Fe_2O_3*	0.77	0.34	1.36	0.89	1.71	1.09	1.28	1.06	1.23
FeO	4.26	4.82	6.41	7.24	8.06	8.85	11.61	14.95	21.01
MgO	21.85	21.49	19.54	19.20	18.47	18.12	15.68	13.61	10.45
MnO	0.16	0.18	0.14	0.11	0.17	0.15	0.45	0.36	0.23
CaO	12.23	11.97	12.67	12.94	12.28	12.38	12.47	12.13	11.48
Na_2O	0.35	0.40	0.54	0.34	0.65	0.50	0.16	0.41	0.13
K_2O	0.04	0.03	0.27	0.27	0.25	0.18	0.03	0.18	0.00
F	0.00	0.01	0.82	0.62	1.04	0.90		0.20	0.04
Cl	0.00	0.00	0.01	0.00	0.00	0.02		0.03	0.07
H_2O†	2.11	2.14	1.66	1.81	1.53	1.64	2.00	1.89	1.86
O=F,Cl	0.00	0.00	0.35	0.26	0.44	0.38	0.00	0.09	0.03
Total	100.27	99.73	100.30	99.94	100.44	99.60	99.69	99.98	100.04
Atoms per formula unit‡									
Si	7.941	7.954	7.785	7.822	7.776	7.836	7.888	7.690	7.997
$^{[4]}$Al	0.059	0.046	0.215	0.178	0.224	0.164	0.112	0.310	0.003
ΣT	8.000	8.000	8.000	8.000	8.000	8.000	8.000	8.000	8.000
$^{[6]}$Al	0.063	0.092	0.038	0.021	0.030	0.014	0.084	0.117	0.006
Ti	0.002	0.000	0.014	0.004	0.010	0.005	0.001	0.013	0.000
Fe^{3+}	0.080	0.036	0.143	0.095	0.181	0.117	0.138	0.116	0.138
Fe^{2+}	0.490	0.558	0.751	0.852	0.952	1.053	1.397	1.826	2.626
Mg	4.481	4.432	4.081	4.031	3.886	3.846	3.362	2.964	2.328
Mn	0.019	0.021	0.017	0.013	0.020	0.018	0.055	0.045	0.029
Σ C	5.135	5.140	5.044	5.016	5.079	5.053	5.037	5.081	5.127
Ca	1.802	1.774	1.902	1.953	1.857	1.888	1.922	1.898	1.838
^{B}Na	0.063	0.087	0.054	0.030	0.065	0.057	0.045	0.021	0.035
Σ B+C	7.000	7.000	7.000	7.000	7.000	7.000	7.000	7.000	7.000
^{A}Na	0.030	0.020	0.092	0.063	0.113	0.080	0.003	0.095	0.003
K	0.007	0.005	0.048	0.048	0.045	0.033	0.005	0.033	0.000
F	0.000	0.004	0.363	0.276	0.464	0.405	0.000	0.092	0.019
Cl	0.000	0.000	0.002	0.000	0.000	0.005	0.000	0.007	0.018
OH	1.940	1.976	1.565	1.696	1.436	1.556	1.920	1.843	1.853
O§	0.060	0.020	0.080	0.028	0.100	0.034	0.080	0.058	0.110

Note: – = untreated.
* Fe^{3+} from Table 2.
† Calculated assuming (OH + F + Cl + O) = 2.000.
‡ Anhydrous oxygen basis of 23.0 O atoms + $X_{oxy\text{-}actinolite}$.
§ See text for calculation method; note that $X_{oxy\text{-}actinolite}$ = O/2.

balanced Fe^{3+} cannot be determined. To be helpful in the present context, analysis of H in our crystals, such as by ion probe, would need to be accurate to ±2% relative).

To arrive at chemical formulae (Table 4), we have assumed that all Fe^{3+} in the high-Fe ferro-actinolite USNM 168215 represents oxy-actinolite (there being virtually no possibility in this specimen for cation-charge balanced Fe^{3+}) and that for the heat-treated samples the percentage of oxy-actinolite component is linearly proportional to their content of ferro-actinolite component. This first approximation is implied at constant T, P, and f_{H_2} by the dehydrogenation equilibrium:

$$Ca_2Fe_5^{2+}Si_8O_{22}(OH)_2 = Ca_2Fe_3^{2+}Fe_2^{3+}Si_8O_{24} + H_2$$

The unheated samples have been normalized to formulae with the assumption that their additional Fe^{3+} (in excess of the amount in the heated equivalent) is related to additional oxy-amphibole component. The corresponding anhydrous oxygen formula bases used ($23.0 + \frac{1}{2}Fe^{3+}_{oxy\text{-}amphibole\ pfu}$) are given in Table 4; they range from 23.01 to 23.07. Our choice of normalization scheme influences not only the total cations per formula unit, but also the assignment of Al to the *T* and *M* sites, calculated percent/cummingtonite solid solution (Fe, Mn, and Mg on M4), and the allocation of Na to the M4 and A sites, and, as a result, the ratio Fe/Mg on M4 from the structure refinement. However, its effect on M1, M2, and M3 site assignments is negligible.

Preparatory to structure refinement, the following assumptions were made for the assignment of atoms among the crystallographically distinct sites: (1) $^{[4]}Al = 8.0 - Si$ per formula unit (pfu) and all $^{[4]}Al$ ordered in T1; (2) $^{[6]}Al$ ($= Al_{total} - {}^{[4]}Al$) and Ti were confined to M2; (3) the scattering factors of Fe were used for Fe, Mn, and Fe^{3+}, and all three were designated as Fe*; (4) the fractionation of Fe* and Mg among the four M cation sites was determined from the refinements; (5) Ca was constrained in M4; (6) $^{M4}Na = 7.0 - Ca - (Mg + Fe^* + Ti + {}^{[6]}Al)$; (7) K and residual Na ($= Na_{total} - {}^{M4}Na$) were assigned to the A site; (8) Cl and F (if any) were assumed to occupy the O3 position.

We tried at the outset to minimize the problem of mul-

TABLE 4—*Continued*

11B	11B	11B	12BA	12BA	44973	44973	ID4-4C	ID4-4C	168215	168215
C46	C28	C41	–	C60	–	C59	–	C51	–	C80
53.56	53.56	53.52	53.09	53.06	51.42	51.34	52.58	52.71	50.96	50.58
0.00	0.00	0.00	0.02	0.02	0.04	0.05	0.02	0.00	0.01	0.04
0.15	0.12	0.09	0.45	0.40	1.69	1.65	0.15	0.15	0.10	0.10
0.97	0.99	0.98	1.69	0.95	2.43	1.48	1.09	1.11	1.03	1.05
20.92	21.27	21.22	20.21	20.54	19.68	20.87	23.52	24.06	29.84	30.51
10.92	10.78	10.73	10.82	10.79	9.13	8.70	8.63	8.53	3.50	2.97
0.21	0.24	0.20	0.34	0.32	2.48	2.65	0.67	0.74	1.43	1.34
11.09	11.16	11.14	11.43	11.69	10.97	10.68	11.15	11.20	11.78	11.57
0.24	0.18	0.19	0.26	0.18	0.37	0.38	0.06	0.06	0.04	0.06
0.01	0.03	0.01	0.04	0.01	0.06	0.06	0.01	0.01	0.11	0.02
0.05	0.05	0.05	0.00	0.05	0.05	0.05	0.01	0.05		0.01
0.07	0.07	0.08	0.00	0.04	0.00	0.00	0.06	0.05		0.01
1.89	1.89	1.88	1.89	1.89	1.83	1.87	1.84	1.86	1.80	1.78
0.04	0.04	0.04	0.00	0.03	0.02	0.02	0.02	0.03	0.00	0.01
100.04	100.30	100.05	100.24	99.92	100.13	99.76	99.77	100.50	100.59	100.13
					Atoms per formula unit‡					
7.985	7.979	7.989	7.911	7.929	7.756	7.790	7.988	7.967	7.974	7.979
0.015	0.021	0.011	0.079	0.071	0.244	0.210	0.012	0.027	0.018	0.019
8.000	8.000	8.000	7.990	8.000	8.000	8.000	8.000	7.994	7.992	7.998
0.011	0.000	0.005	0.000	0.000	0.056	0.085	0.014	0.000	0.000	0.000
0.000	0.000	0.000	0.002	0.002	0.004	0.006	0.002	0.000	0.001	0.005
0.109	0.110	0.110	0.190	0.107	0.276	0.169	0.124	0.127	0.121	0.124
2.608	2.650	2.649	2.518	2.567	2.483	2.648	2.988	3.041	3.904	4.025
2.427	2.394	2.388	2.403	2.404	2.053	1.968	1.954	1.922	0.816	0.700
0.026	0.030	0.025	0.043	0.040	0.317	0.341	0.086	0.095	0.190	0.179
5.181	5.184	5.177	5.146	5.120	5.189	5.217	5.168	5.178	5.024	5.030
1.771	1.781	1.782	1.825	1.872	1.773	1.736	1.815	1.814	1.975	1.956
0.048	0.034	0.041	0.029	0.007	0.038	0.048	0.015	0.018	0.001	0.015
7.000	7.000	7.000	7.000	7.000	7.000	7.000	7.000	7.000	7.000	7.000
0.021	0.018	0.014	0.046	0.045	0.070	0.064	0.002	0.010	0.011	0.003
0.002	0.006	0.002	0.008	0.002	0.011	0.012	0.002	0.002	0.022	0.024
0.023	0.023	0.024	0.000	0.024	0.024	0.024	0.005	0.024	0.000	0.005
0.018	0.018	0.020	0.000	0.010	0.000	0.000	0.015	0.013	0.000	0.003
1.879	1.879	1.876	1.880	1.886	1.836	1.894	1.860	1.871	1.880	1.868
0.080	0.080	0.080	0.120	0.080	0.140	0.082	0.120	0.092	0.120	0.124

tiple occupancy of M sites, namely by Ti^{4+}, Al^{3+}, Fe^{3+}, and Mn^{2+} in addition to Fe^{2+} and Mg, through our selection of samples, but we were not entirely successful. Fortunately, Ti is present near the detection limits (Table 4), and the amounts of Al are low enough to rule out significant disorder on both *M* and *T* sites (Oberti et al. 1995a, 1995b), particularly in light of relatively low crystallization and equilibration temperatures. However, the site preferences of Fe^{3+} and Mn are more problematic, as discussed in the section "M-site fractionation of Fe^{2+} and Mg."

Structure refinements were done on two crystals for each of nine samples, one untreated, and the other equilibrated at high temperature (Table 2) and quenched prior to X-ray examination. All refinements were carried out based on the space group *C*2/*m*, and procedures for the refinements are similar to those described by Hirschmann et al. (1994). During all cycles of refinement, chemical compositions were required to match those determined from electron microprobe analysis. Some refinements were also undertaken using the split M4- and A-site models to test their influence on the refined site occupancies. The resulting Fe*/(Fe* + Mg) ratios for the four M sites were not significantly different from those based on the unsplit M4- and A-site model. Hence, only the refinement results performed with the unsplit M4- and A-site model are presented here. Final atomic positional coordinates and anisotropic displacement parameters are listed in Tables 5[1] and 6[1], respectively. Selected bond distances are given in Table 7 and angles in Table 8.

RESULTS AND DISCUSSION

Crystal chemistry

The replacement of Mg and Fe by Ca in quadrilateral clinoamphiboles induces major changes in the geometry of the M4-O polyhedron, from an irregular 4 + 2 octahedron in the cummingtonite series to an eightfold-coordinated polyhedron in the actinolite series. As evidenced in natural parageneses and experiments (Cameron 1975), the resulting miscibility gap between the two series is wide and fails to close prior to thermal decomposition to pyroxene, quartz, and H_2O. Because this work greatly expands the crystallographic database for the actinolite series, our discussion here focuses on the comparative crystal chemistry of quadrilateral clinoamphiboles and its relevance to the ordering of cations on the M sites.

In *C*2/*m* clinoamphiboles the mean bond lengths, ⟨Mi-O⟩, of the M1, M2, and M3 octahedra vary linearly with

TABLE 7. Interatomic distances (Å) in actinolite series samples

	93728	C78	67-3172	C70	67-3701	C71	156831	C79	11B
M1-O1 (×2)	2.069(2)	2.067(2)	2.067(1)	2.070(1)	2.072(3)	2.070(1)	2.083(2)	2.082(3)	2.091(3)
M1-O2 (×2)	2.088(2)	2.091(2)	2.085(2)	2.080(2)	2.084(4)	2.079(2)	2.099(2)	2.102(4)	2.111(4)
M1-O3 (×2)	2.091(2)	2.088(2)	2.086(1)	2.086(1)	2.086(5)	2.091(1)	2.104(2)	2.099(3)	2.120(3)
Avg.	2.083	2.082	2.080	2.079	2.081	2.080	2.095	2.094	2.107
M2-O1 (×2)	2.134(2)	2.140(2)	2.141(2)	2.144(2)	2.141(4)	2.147(2)	2.143(2)	2.146(4)	2.157(4)
M2-O2 (×2)	2.088(2)	2.089(2)	2.093(1)	2.102(1)	2.097(3)	2.102(1)	2.103(2)	2.107(3)	2.118(3)
M2-O4 (×2)	2.016(2)	2.020(2)	2.014(2)	2.016(1)	2.014(4)	2.019(2)	2.019(2)	2.022(4)	2.028(4)
Avg.	2.080	2.083	2.083	2.087	2.084	2.089	2.088	2.092	2.101
M3-O1 (×4)	2.079(2)	2.078(2)	2.075(2)	2.071(2)	2.082(3)	2.074(2)	2.086(2)	2.088(3)	2.100(3)
M3-O3 (×2)	2.061(3)	2.063(3)	2.062(2)	2.065(2)	2.058(7)	2.063(2)	2.079(3)	2.070(5)	2.083(5)
Avg.	2.073	2.073	2.071	2.069	2.074	2.070	2.084	2.082	2.094
M4-O2 (×2)	2.389(2)	2.388(2)	2.399(2)	2.398(2)	2.406(4)	2.400(2)	2.399(2)	2.400(4)	2.386(4)
M4-O4 (×2)	2.305(2)	2.304(2)	2.324(1)	2.326(1)	2.319(3)	2.323(1)	2.323(2)	2.321(3)	2.299(3)
M4-O5 (×2)	2.781(2)	2.793(2)	2.769(2)	2.773(1)	2.765(4)	2.777(2)	2.783(2)	2.777(3)	2.839(3)
M4-O6 (×2)	2.552(2)	2.556(2)	2.544(2)	2.544(2)	2.549(4)	2.547(2)	2.547(2)	2.549(4)	2.567(4)
Avg.	2.507	2.510	2.509	2.510	2.510	2.512	2.513	2.512	2.523
T1-O1	1.608(2)	1.607(2)	1.610(1)	1.607(1)	1.608(3)	1.611(1)	1.610(2)	1.609(3)	1.602(3)
T1-O5	1.635(2)	1.635(2)	1.636(2)	1.635(1)	1.645(4)	1.637(2)	1.637(2)	1.647(4)	1.633(4)
T1-O6	1.634(2)	1.630(2)	1.640(2)	1.635(1)	1.641(4)	1.637(2)	1.638(2)	1.643(3)	1.632(3)
T1-O7	1.620(1)	1.622(1)	1.622(1)	1.620(1)	1.622(2)	1.623(1)	1.623(1)	1.627(2)	1.622(2)
Avg.	1.624	1.624	1.627	1.624	1.629	1.627	1.627	1.631	1.622
T2-O2	1.617(2)	1.615(2)	1.615(1)	1.611(1)	1.617(3)	1.615(1)	1.619(2)	1.617(3)	1.608(3)
T2-O4	1.591(2)	1.587(2)	1.590(2)	1.585(2)	1.594(4)	1.586(2)	1.585(2)	1.588(4)	1.585(4)
T2-O5	1.656(2)	1.654(2)	1.654(2)	1.653(1)	1.651(4)	1.655(2)	1.659(2)	1.656(3)	1.657(3)
T2-O6	1.676(2)	1.676(2)	1.670(2)	1.671(1)	1.672(4)	1.671(2)	1.673(2)	1.680(3)	1.673(4)
Avg.	1.635	1.633	1.632	1.630	1.633	1.632	1.634	1.635	1.631

$\langle r_{Mi} \rangle$, the average effective radius of the cations occupying individual sites (Robinson et al. 1973; Hawthorne 1978, 1983). These relationships provide constraints on site occupancies in addition to those derived from site-scattering refinements, and they provide a measure of mean bond lengths (M-O volumes) for given mean ionic radii. For cummingtonite and grunerite, the experimental data of Hirschmann et al. (1994) agree well with the relationships given by Hawthorne (1983), although it should be pointed out that Hirschmann et al. (1994) adopted a radius of 0.77 Å for Fe^{2+} (Shannon and Prewitt 1969) in their regressions. For consistency with the study of Hawthorne (1983), we use a radius of 0.78 Å for Fe^{2+} (Shannon 1976) and have recalculated all the $\langle r_{Mi} \rangle$ values for octahedral sites in 30 cummingtonite and grunerite crystals studied by Hirschmann et al. (1994). The relationships for ferromagnesian clinoamphibole are:

$$\langle M1-O \rangle = 1.479 + 0.839\langle r_{M1} \rangle \qquad R^2 = 0.97$$

$$\langle M2-O \rangle = 1.462 + 0.864\langle r_{M2} \rangle \qquad R^2 = 0.97$$

$$\langle M3-O \rangle = 1.434 + 0.888\langle r_{M3} \rangle \qquad R^2 = 0.96$$

$$\langle M123-O \rangle = 1.456 + 0.867\langle r_{M123} \rangle \qquad R^2 = 0.98$$

By combining our data (Table 7) with those reported previously for ferro-actinolite (Mitchell et al. 1970) and tremolite (Papike et al. 1969; Yang and Evans 1996), linear regression yields the following relationships between $\langle Mi\text{-}O \rangle$ and $\langle r_{Mi} \rangle$ for the M1, M2, and M3 octahedral sites in the actinolite series:

$$\langle M1-O \rangle = 1.471 + 0.838\langle r_{M1} \rangle \qquad R^2 = 0.96$$

$$\langle M2-O \rangle = 1.527 + 0.774\langle r_{M2} \rangle \qquad R^2 = 0.96$$

$$\langle M3-O \rangle = 1.449 + 0.857\langle r_{M3} \rangle \qquad R^2 = 0.96$$

$$\langle M123-O \rangle = 1.476 + 0.831\langle r_{M123} \rangle \qquad R^2 = 0.98$$

For $\langle r_{Mi} \rangle$ between 0.72 and 0.78 Å, both $\langle M1\text{-}O \rangle$ and $\langle M3\text{-}O \rangle$ values determined for the actinolite series are systematically smaller (by 0.005 to 0.010 Å) than those we would obtain from the equations of Hawthorne (1983) for *C*2/*m* amphiboles and Hirschmann et al. (1994) for cummingtonite-grunerite (Fig. 1). For $\langle M2\text{-}O \rangle$, our fit incorporates values of $\langle r_{M2} \rangle$ based on Fe^{3+} and Fe^{2+} derived in part from the equation of Hawthorne (1983), as discussed earlier. Nonetheless, it appears that in the actinolite series, for a given $\langle r_{Mi} \rangle$, the relative sizes of the octahedra are: M2-O> M1-O> M3-O. In the unlikely case that all Fe on M2 is Fe^{2+}, the difference between $\langle M2\text{-}O \rangle$ and $\langle M1\text{-}O \rangle$ is reduced but not eliminated. In cummingtonite-grunerite the M1 and M2 sites have indistinguishable mean bond lengths (Hirschmann et al. 1994). The preference of Al^{3+} for the M2 site in aluminous calcic amphiboles must therefore be related to factors other than site dimension (see below).

Examination of individual M-O bond lengths shows that the shorter $\langle M1\text{-}O \rangle$ and $\langle M3\text{-}O \rangle$ distances for the actinolite series, for a given $\langle r_{Mi} \rangle$ value, are due to significant shortening of the M1-O2 and M3-O1 bond distances relative to those in cummingtonite-grunerite. For a given $\langle r \rangle$ value, the M1-O2 and M3-O1 bond lengths in the

[1] For a copy of Tables 5 and 6, Document AM-98-009, contact the Business Office of the Mineralogical Society of America (see inside front cover of recent issue) for price information. Deposit items may also be available on the *American Mineralogist* web site at http://www.minsocam.org.

TABLE 7—*Continued*

C46	C28	C41	12BA	C60	44973	C59	ID4-4C	C51	168215	C80
2.087(1)	2.089(1)	2.087(1)	2.091(2)	2.088(1)	2.088(2)	2.087(1)	2.098(3)	2.092(1)	2.114(3)	2.107(3)
2.106(2)	2.106(2)	2.105(2)	2.106(2)	2.105(2)	2.114(2)	2.109(2)	2.117(4)	2.108(2)	2.123(3)	2.122(4)
2.111(1)	2.110(1)	2.110(1)	2.110(2)	2.112(1)	2.113(1)	2.113(1)	2.118(3)	2.113(1)	2.125(3)	2.123(4)
2.101	2.102	2.101	2.103	2.101	2.105	2.103	2.111	2.104	2.120	2.117
2.157(2)	2.158(2)	2.158(2)	2.154(2)	2.160(2)	2.150(2)	2.159(2)	2.160(4)	2.161(2)	2.172(3)	2.175(4)
2.119(1)	2.120(1)	2.121(1)	2.117(2)	2.124(1)	2.113(1)	2.122(1)	2.152(3)	2.130(1)	2.147(3)	2.147(3)
2.026(1)	2.029(1)	2.028(1)	2.023(2)	2.027(2)	2.022(2)	2.026(2)	2.029(4)	2.033(2)	2.043(3)	2.043(4)
2.100	2.102	2.102	2.098	2.104	2.095	2.102	2.104	2.108	2.121	2.122
2.095(2)	2.094(2)	2.094(2)	2.090(2)	2.094(2)	2.098(2)	2.092(2)	2.107(3)	2.096(2)	2.109(3)	2.114(3)
2.082(2)	2.084(2)	2.083(1)	2.085(3)	2.082(2)	2.084(2)	2.084(2)	2.090(5)	2.091(2)	2.095(4)	2.102(5)
2.091	2.091	2.090	2.089	2.090	2.094	2.090	2.101	2.094	2.104	2.110
2.384(2)	2.384(2)	2.381(2)	2.379(2)	2.386(2)	2.382(2)	2.382(2)	2.380(4)	2.381(2)	2.399(4)	2.401(4)
2.302(1)	2.303(1)	2.302(1)	2.306(2)	2.309(1)	2.303(2)	2.302(1)	2.303(3)	2.302(1)	2.322(3)	2.317(3)
2.832(1)	2.835(1)	2.838(1)	2.832(2)	2.828(1)	2.819(2)	2.821(1)	2.834(3)	2.842(1)	2.841(3)	2.842(3)
2.568(2)	2.571(2)	2.571(2)	2.566(2)	2.568(2)	2.562(2)	2.572(2)	2.571(4)	2.573(2)	2.569(4)	2.572(4)
2.522	2.523	2.522	2.521	2.523	2.517	2.519	2.522	2.525	2.533	2.533
1.609(1)	1.609(1)	1.608(1)	1.609(2)	1.610(1)	1.615(2)	1.614(1)	1.600(3)	1.608(1)	1.600(3)	1.604(3)
1.632(1)	1.634(1)	1.632(1)	1.635(2)	1.637(1)	1.640(2)	1.640(1)	1.628(4)	1.635(1)	1.633(3)	1.631(4)
1.634(1)	1.633(1)	1.633(1)	1.633(2)	1.637(1)	1.640(2)	1.641(1)	1.637(3)	1.635(1)	1.642(3)	1.640(4)
1.622(1)	1.620(1)	1.620(0)	1.619(1)	1.619(1)	1.623(1)	1.624(1)	1.619(2)	1.620(1)	1.621(2)	1.620(2)
1.624	1.624	1.623	1.624	1.626	1.630	1.630	1.621	1.624	1.624	1.624
1.615(1)	1.613(1)	1.614(1)	1.613(2)	1.614(1)	1.617(1)	1.615(1)	1.613(3)	1.610(1)	1.610(3)	1.615(3)
1.591(2)	1.589(2)	1.590(2)	1.585(2)	1.587(2)	1.590(2)	1.591(2)	1.587(4)	1.587(2)	1.581(4)	1.586(4)
1.656(1)	1.658(1)	1.656(1)	1.654(2)	1.657(1)	1.651(2)	1.655(1)	1.666(3)	1.653(1)	1.666(3)	1.663(4)
1.671(1)	1.674(1)	1.673(1)	1.670(2)	1.673(1)	1.668(2)	1.670(1)	1.674(4)	1.673(1)	1.676(3)	1.675(4)
1.634	1.633	1.633	1.631	1.633	1.632	1.633	1.635	1.631	1.633	1.635

actinolite series are 0.044 and 0.015 Å shorter than the corresponding bonds in cummingtonite-grunerite. As a result, the M1 and M3 octahedra in the former are slightly more regular than those in the latter in terms of quadratic elongation (Robinson et al. 1971). Among the M1, M2, and M3 octahedra in the actinolite series, M3 shows the largest angular deviation from a perfect octahedron and M2 the smallest (Table 9). With increasing macroscopic X_{Fe} [= Fe/(Fe+Mg)], the angular distortions of all three octahedra decrease, in contrast to cummingtonite-grunerite in which the angular distortions of the M2 and M3 octahedra increase considerably (Hirschmann et al. 1994).

There is no apparent correlation between ⟨M4-O⟩ and $\langle r_{M4} \rangle$ in the actinolite series. Similar observations were made by Hawthorne (1983) and Hirschmann et al. (1994) for *C*2/*m* amphiboles and cummingtonite-grunerite, respectively. However, ⟨M4-O⟩ appears to be a function of macroscopic X_{Fe} (Fig. 2). The increase in ⟨M4-O⟩ with increase in macroscopic X_{Fe} results principally from the lengthening of the two longer distances M4-O5 and M4-O6, because the two shorter distances M4-O2 and M4-O4 are virtually independent of macroscopic X_{Fe}. Because O5 and O6 are the bridging atoms of the silicate chains, the above observation indicates that the variation in ⟨M4-O⟩ depends strongly on the configuration of the silicate chains, which in turn is correlated with changes in the octahedral strips. In other words, the variation in ⟨M4-O⟩ is strongly subject to change in the rest of the structure.

TABLE 8. Selected interatomic bond angles in actinolite series samples

Specimen no.	O5-O6-O5	O5-O7-O6	T1-O5-T2	T1-O6-T2	T1-O7-T1
NMNH 93728	167.6(1)	166.7(1)	136.4(1)	138.3(1)	139.6(2)
C78	167.8(1)	166.9(1)	136.7(1)	138.3(1)	139.2(2)
67-3172	167.7(1)	166.7(1)	136.6(1)	138.1(1)	139.1(1)
C70	167.9(1)	166.9(1)	136.8(1)	138.3(1)	139.1(1)
67-3701	167.1(2)	166.8(2)	136.3(2)	138.0(2)	139.5(3)
C71	167.9(1)	166.9(1)	136.7(1)	138.2(1)	138.9(1)
NMNH 156831	168.3(1)	167.0(1)	137.0(1)	138.9(1)	140.1(2)
C79	167.5(2)	166.6(2)	136.4(2)	138.0(2)	140.0(3)
11B	169.1(2)	168.2(2)	137.4(2)	138.9(2)	140.5(3)
C46	168.8(1)	167.9(1)	137.4(1)	139.0(1)	140.6(1)
C28	168.7(1)	168.0(1)	137.2(1)	138.7(1)	140.7(1)
C41	168.7(1)	167.9(1)	137.3(1)	138.8(1)	140.5(1)
12BA	168.9(1)	167.9(1)	137.6(1)	139.1(1)	140.7(2)
C60	168.7(1)	168.0(1)	137.3(1)	138.9(1)	140.8(1)
AMNH 44973	168.4(1)	167.6(1)	137.4(1)	139.1(1)	140.5(1)
C59	168.1(1)	167.0(1)	137.3(1)	138.8(1)	140.4(1)
ID4-4C	169.0(2)	167.9(2)	137.4(2)	138.8(2)	141.2(3)
C51	168.8(1)	168.1(1)	137.6(1)	138.8(1)	140.9(1)
NMNH 168215	169.5(2)	168.6(2)	137.6(2)	138.6(2)	141.2(3)
C80	169.5(2)	168.5(2)	137.7(2)	138.6(2)	141.5(3)

The mean tetrahedral bond lengths of the T1 and T2 tetrahedra, ⟨T1-O⟩ and ⟨T2-O⟩, do not correlate with macroscopic X_{Fe}; ⟨T1-O⟩ ranges from 1.620 to 1.631 Å with an average value of 1.625(2) Å and ⟨T2-O⟩ from 1.630 to 1.635 Å with an average value of 1.633(1) Å. The correlation between $^{[4]}$Al from microprobe analysis (Table 4) and ⟨T1-O⟩ (Fig. 3) shows that the larger variation in ⟨T1-O⟩ stems from the preference of Al for the T1 site over the T2 site, as discussed in detail by Oberti et al. (1995b). The average ⟨T1-O⟩ and ⟨T2-O⟩ distances in the actinolite series are both longer than the corresponding distances [1.620(1) Å for ⟨T1-O⟩ and 1.628(1) Å for ⟨T2-O⟩] in cummingtonite-grunerite. A comparison of individual T-O bond lengths shows that the longer ⟨T1-O⟩ and ⟨T2-O⟩ distances for the actinolite series primarily result from the large differences in the T-O5 and T-O6 bond lengths. The average T1-O5, T1-O6, T2-O5, and T2-O6 bond distances in the actinolite series are 1.636(3),

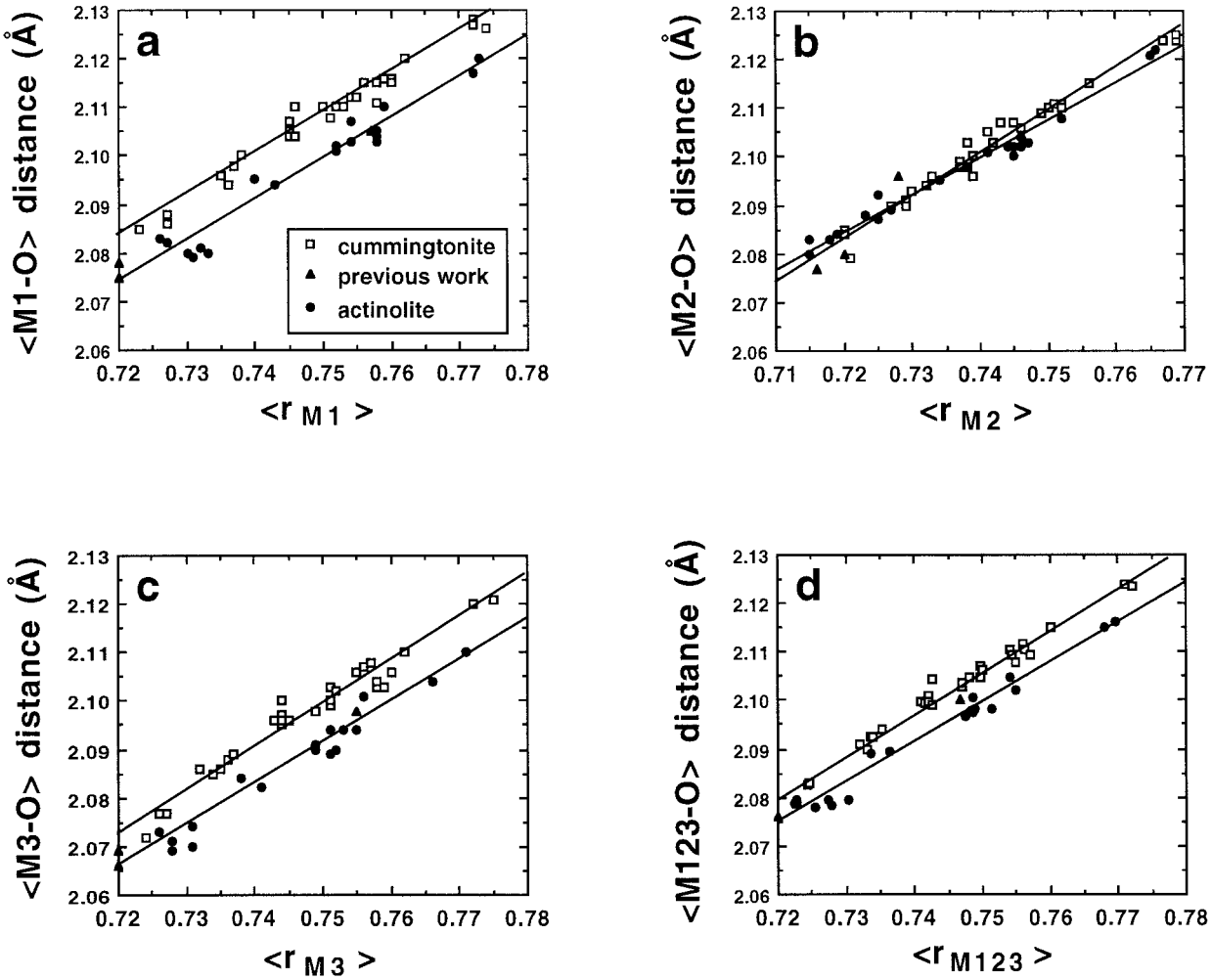

FIGURE 1. Correlation between mean bond length and mean cation radius for the actinolite and cummingtonite series. Actinolites (filled circles) this work; cummingtonite-grunerite (open squares) from Hirschmann et al. (1994); previous work (filled triangles) = tremolite from Papike et al. (1969) and Yang and Evans (1996); and ferro-actinolite from Mitchell et al. (1970, 1971).

1.637(3), 1.655(4), and 1.671(5) Å, respectively, whereas in cummingtonite-grunerite they are 1.619(2), 1.626(2), 1.634(2), and 1.649(2) Å. In all samples studied here, the T1 tetrahedron is much less distorted than T2, as measured by the tetrahedral quadratic elongation (TQE) and angle variance (TAV). Similar to the three MO_6 octahedra, the angular distortions of both T1 and T2 tetrahedra, which become less distorted with increasing macroscopic X_{Fe}, appear to be correlated with the configuration of the silicate chains in that the chains become straighter (measured by the O5-O6-O5 kinking angle) and wider (measured by the T1-O7-T1 angle) with increasing macroscopic X_{Fe} (Table 9). The O5-O6-O5 angle ranges from 167.5° in tremolite to 169.5° in the ferro-actinolite C80, whereas in cummingtonite-grunerite the O5-O6-O5 angle (~171°) is essentially independent of composition (Yang and Hirschmann 1995).

Despite their fundamental structural similarity, several differences between the cummingtonite and actinolite series structures are apparent, as described above. From the crystal-chemical viewpoint, these structural differences can be rationalized in terms of the bond-valence model. For comparison purposes we choose ferro-actinolite 12BA (this study) and grunerite 2b (Hirschmann et al. 1994) for the bond-valence calculation, because these two samples show similar Fe-Mg site occupancies in the M1, M2, and M3 sites and differ mainly in the cations occupying the M4 site. For simplicity, the trace amount of cations in the A site in sample 12BA were ignored in the calculation. Bond-valence arrangements for the two samples (Table 10) were calculated using the curve of Brown (1981). One of the most marked differences resulting from the substitution of Ca in ferro-actinolite for (Fe+Mg) in grunerite is the significant change in the bond-valence distribution around the M4 site. Specifically, the bond-valence distributions from M4 to O2 and O4 are decreased considerably and those from M4 to O5 and O6 are increased. The direct impact of such changes on

TABLE 9. Distortion indices for polyhedra in actinolite series samples

Specimen no.	Parameter	M1	M2	M3	M4	T1	T2
NMNH 93728	*V*	11.86(1)	11.87(1)	11.64(2)	26.08(2)	2.195(4)	2.227(4)
	QE	1.011(1)	1.007(1)	1.014(1)		1.001(1)	1.005(1)
	AV	35.1(2)	22.3(2)	44.3(2)		4.9(1)	20.6(2)
C78	*V*	11.84(1)	11.93(1)	11.65(2)	26.18(2)	2.193(4)	2.219(4)
	QE	1.010(1)	1.007(1)	1.013(1)		1.001(1)	1.005(1)
	AV	34.4(2)	22.6(2)	43.7(2)		4.6(1)	20.2(2)
67-3172	*V*	11.80(1)	11.92(1)	11.60(1)	26.23(2)	2.206(3)	2.216(3)
	QE	1.011(1)	1.008(1)	1.014(1)		1.001(1)	1.005(1)
	AV	36.1(1)	23.8(1)	45.0(1)		4.8(1)	19.9(2)
C70	*V*	11.79(1)	11.99(1)	11.58(1)	26.24(1)	2.195(2)	2.207(3)
	QE	1.011(1)	1.008(1)	1.013(1)		1.001(1)	1.005(1)
	AV	35.0(1)	24.5(1)	43.8(1)		4.7(1)	20.1(2)
67-3701	*V*	11.81(3)	11.95(2)	11.65(4)	26.26(4)	2.215(6)	2.221(7)
	QE	1.011(3)	1.007(2)	1.014(3)		1.001(1)	1.005(2)
	AV	37.0(4)	23.3(2)	46.3(4)		5.1(2)	20.4(4)
C71	*V*	11.81(1)	12.03(1)	11.60(1)	26.29(2)	2.207(3)	2.214(3)
	QE	1.011(1)	1.008(1)	1.013(1)		1.001(3)	1.005(1)
	AV	35.1(1)	24.6(1)	43.6(1)		5.1(1)	20.4(2)
NMNH 156831	*V*	12.08(1)	12.02(1)	11.82(2)	26.33(2)	2.207(3)	2.224(4)
	QE	1.011(1)	1.007(1)	1.014(1)		1.001(5)	1.005(1)
	AV	34.8(2)	23.0(1)	44.8(2)		4.2(1)	20.2(2)
C79	*V*	12.04(2)	12.08(2)	11.79(3)	26.30(4)	2.224(6)	2.227(7)
	QE	1.011(2)	1.007(2)	1.014(2)		1.001(1)	1.005(2)
	AV	36.7(3)	22.4(2)	46.1(4)		5.4(2)	20.0(4)
11B	*V*	12.30(2)	12.25(2)	12.02(3)	26.57(4)	2.188(6)	2.211(7)
	QE	1.009(2)	1.007(2)	1.013(2)		1.001(1)	1.006(2)
	AV	31.2(3)	22.0(2)	41.9(3)		3.9(2)	19.1(4)
C46	*V*	12.19(1)	12.23(1)	11.95(1)	26.53(2)	2.196(2)	2.224(3)
	QE	1.010(1)	1.008(1)	1.013(1)		1.001(1)	1.006(1)
	AV	33.0(1)	23.3(1)	44.0(1)		3.6(1)	17.8(2)
C28	*V*	12.20(1)	12.26(1)	11.95(1)	26.56(2)	2.195(2)	2.223(3)
	QE	1.010(1)	1.008(1)	1.013(1)		1.001(1)	1.005(1)
	AV	32.6(1)	23.4(1)	43.4(1)		3.8(1)	17.7(2)
C41	*V*	12.18(1)	12.26(1)	11.94(1)	26.54(2)	2.193(2)	2.222(3)
	QE	1.010(1)	1.007(1)	1.013(1)		1.001(1)	1.005(1)
	AV	32.7(1)	23.2(1)	43.4(1)		3.8(1)	17.3(2)
12BA	*V*	12.23(2)	12.19(1)	11.91(2)	26.51(2)	2.196(4)	2.211(4)
	QE	1.010(1)	1.008(1)	1.013(1)		1.001(1)	1.005(1)
	AV	33.3(2)	23.2(1)	43.4(2)		3.2(1)	18.3(2)
C60	*V*	12.19(1)	12.29(1)	11.93(1)	26.57(2)	2.202(2)	2.219(3)
	QE	1.010(1)	1.008(1)	1.013(1)		1.001(1)	1.005(1)
	AV	33.0(1)	23.6(1)	43.2(1)		3.7(1)	18.5(2)
AMNH 44973	*V*	12.24(1)	12.14(1)	11.98(1)	26.42(2)	2.218(3)	2.216(3)
	QE	1.011(1)	1.007(1)	1.014(1)		1.001(1)	1.005(1)
	AV	35.0(1)	22.6(1)	47.0(2)		3.3(1)	17.1(2)
C59	*V*	12.21(1)	12.26(1)	11.92(1)	26.48(2)	2.219(2)	2.220(3)
	QE	1.010(1)	1.008(1)	1.014(1)		1.001(1)	1.004(1)
	AV	34.2(1)	23.4(1)	45.0(1)		3.4(1)	17.1(2)
ID4-4C	*V*	12.35(2)	12.29(2)	12.13(3)	26.52(4)	2.181(6)	2.226(7)
	QE	1.010(2)	1.007(2)	1.013(2)		1.001(1)	1.005(2)
	AV	32.2(3)	21.3(2)	42.7(3)		4.0(2)	18.4(4)
C51	*V*	12.24(1)	12.37(1)	12.01(1)	26.61(2)	2.197(2)	2.212(3)
	QE	1.010(1)	1.007(1)	1.013(1)		1.001(1)	1.005(1)
	AV	32.1(1)	23.1(1)	43.2(1)		3.4(1)	18.0(2)
NMNH 168215	*V*	12.53(2)	12.59(2)	12.19(3)	26.91(4)	2.195(5)	2.221(6)
	QE	1.010(2)	1.007(1)	1.013(2)		1.001(1)	1.005(2)
	AV	32.2(3)	22.5(2)	41.4(3)		4.6(2)	18.7(4)
C80	*V*	12.48(2)	12.62(2)	12.29(3)	26.93(4)	2.195(6)	2.228(7)
	QE	1.009(2)	1.007(2)	1.013(2)		1.001(1)	1.005(2)
	AV	31.4(3)	22.5(2)	42.2(3)		4.3(2)	18.7(4)

Note: V = polyhedral volume; QE = quadratic elongation; AV = angle variance (Robinson et al. 1971).

the actinolite structure is the pronounced shortening of the M1-O2 and M2-O4 bond distances relative to those in cummingtonite-grunerite, and significant elongation of the T-O5 and T-O6 bond lengths as a consequence of compensation of the bond valence for these four O atoms (O2, O4, O5, and O6). The shortening of the M3-O1 bond distance in actinolite compared with that in cummingtonite-grunerite is an inductive effect due to the reduced bond valence of the M1-O1 bond (to meet the bond-valence requirement for O1), which in turn results from the increased bond valence for the M1-O2 bond (to satisfy the bond-valence requirement for O2). According to Hawthorne (1983), the increase in the bond valences for the M4-O5 and M4-O6 bonds is one of the major factors affecting the distribution of bond valences in the tetrahedral double chains and responsible for the increased O-

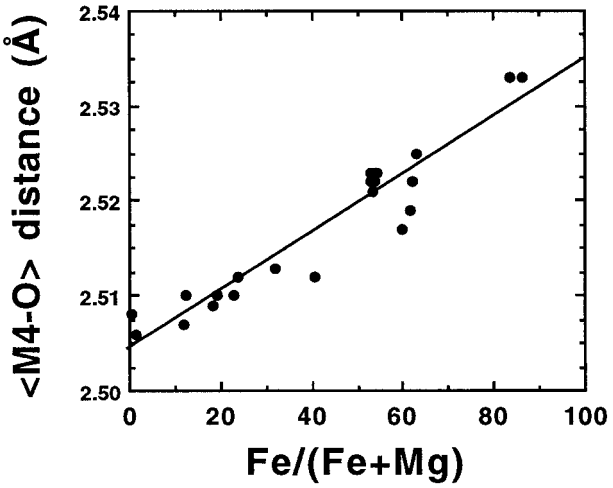

FIGURE 2. Correlation between mean bond length <M4-O> and macroscopic X_{Fe} in the actinolite series.

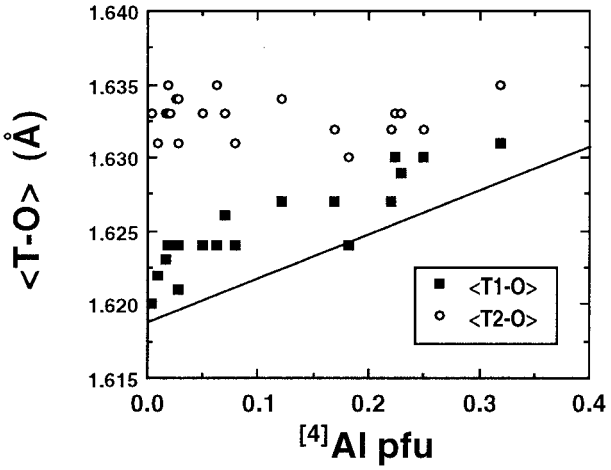

FIGURE 3. Mean tetrahedral bond lengths in the actinolite series as a function of [4]Al: Filled squares = ⟨T1-O⟩, open circles = ⟨T2-O⟩. Straight line = fit to the Pavia database of amphiboles (Oberti et al. 1995b).

rotation of the silicate chains. This conclusion is supported by our data; the O5-O6-O5 kinking angle in the actinolite series is always smaller than that in *C*2/*m* cummingtonite-grunerite.

Another noticeable difference in the bond-valence arrangement for the two series is the appreciable decrease in the summed bond valence for O4 (1.883 against 1.945 v.u. for cummingtonite) that is already strongly deficient relative to the ideal value of 2.0 v.u. As O4 is bonded to M2, M4, and T2, our results suggest that, given the same conditions, the M2 site in the actinolite series is more favored by higher-valence cations than M2 in cummingtonite-grunerite, to maintain a high bond-valence value for O4, despite the fact that ⟨M2-O⟩ in actinolite is longer than ⟨M1-O⟩ and ⟨M3-O⟩. Hawthorne (1983) and Oberti et al. (1995b) also attributed the ordering of Al in the T1 site to the deficiency of the bond valence for O4 because any Al at T2 will further reduce the bond valence of O4.

M-site fractionation of Fe^{2+} and Mg

Because our goal is to evaluate the site preferences of Fe^{2+} and Mg on the four M sites in the actinolite series, and the refinements provide Fe* (= Fe^{2+} + Fe^{3+} + Mn), we must first assess the likely locations of Mn and Fe^{3+}.

Manganese is only a problem in this respect in two samples (AMNH 44973 and NMNH 168215, and their heated equivalents), because Mn in all others constitutes less than 0.05 atoms pfu (Table 4). Based on considerations of cation size and data on manganoan cummingtonite (Papike et al. 1969), previous authors (e.g., Mitchell et al. 1971; Hawthorne 1983; Skogby and Annersten 1985) assumed that all Mn occurs on the M4 site in calcic amphiboles (see also McGavin et al. 1982). Recently, evidence has been presented (Oberti et al. 1993b) for strong ordering of Mn^{2+} on M2 as well as M4 in manganoan richterite. The two refinements done on our most Mn-rich

TABLE 10. Bond-valence table for ferro-actinolite (upper set) and grunerite (lower set)

	M1	M2	M3	M4	T1	T2	Σ
O1	0.368 ×2↓	0.315 ×2↓	0.366 ×4↓		1.035		2.084
O1	0.382 ×2↓	0.310 ×2↓	0.348 ×4↓		1.013		2.053
O2	0.355 ×2↓	0.344 ×2↓		0.294 ×2↓		1.024	2.017
O2	0.319 ×2↓	0.350 ×2↓		0.344 ×2↓		0.989	2.002
O3	0.352 ×2↓→		0.371 ×2↓				1.075
O3	0.352 ×2↓→		0.376 ×2↓				1.080
O4		0.431 ×2↓		0.348 ×2↓		1.104	1.883
O4		0.388 ×2↓		0.511 ×2↓		1.046	1.945
O5				0.113 ×2↓	0.966	0.920	1.999
O5				0.038 ×2↓	1.005	0.971	2.014
O6				0.196 ×2↓	0.971	0.882	2.049
O6				0.096 ×2↓	0.987	0.932	2.015
O7					1.008 ×2→		2.016
O7					1.011 ×2→		2.022
Σ	2.148	2.180	2.206	1.902	3.981	3.930	
Σ	2.106	2.098	2.144	1.976	4.016	3.939	

Note: The ferro-actinolite and grunerite samples used in the calculation are 12BA from this study and 2b from Hirschmann et al. (1994). Arrows determine whether to add across or down or both.

crystals (AMNH 44973 and C59) allow only 0.15 and 0.17 atoms of Fe* pfu on M4, whereas 0.32 and 0.34 Mn atoms pfu, respectively, are present according to the microprobe analyses. Thus, in these samples, at least one-half of the Mn must reside on one or more of the M1, M2, and M3 sites. In fact, to achieve any consistency at all in $Fe^{2+}/(Fe^{2+} + Mg)$ ratio on M4 relative to M1-3 between these samples and all the others (see below) requires most of the Fe* on M4 to be Fe^{2+}; this implies that nearly all Mn must reside on M1, M2, or M3. Furthermore, consistency in partitioning of Fe^{2+} and Mg among the M1-3 sites in heat-treated manganoan ferroactinolite (C59) with those of compositionally similar but low-Mn heated ferro-actinolites (see below) can be brought about by assuming zero Mn on M3 and an Mn/Fe ratio on both M4 and M2 three times larger than the Mn/Fe ratio on M1. This assignment of Mn, although nothing more than an intelligent guess, reflects relative mean bond-lengths in the actinolite series and known preferences in other amphibole groups, and was adopted for all samples in this study.

Because dehydrogenation creates local charge-imbalance at the O3 site, calcic amphiboles with appreciable oxy-amphibole content, that is, strongly dehydrogenated, are believed to have Fe^{3+} on the M1 and M3 sites (Ghose, 1965; Ungaretti et al. 1983; Phillips et al. 1988, 1989), or more precisely, first on M1 and then on M3 (Zanetti et al. 1997; R. Oberti, personal communication). Infrared spectra of ferro-actinolites have been interpreted as showing some Fe^{3+} on M1 + M3, although there is a question of possible oxidation during sample preparation (Burns and Greaves 1971). On the other hand, ferric iron charge-balanced against other cations (^{B}Na or ^{T}Al) enters M2 along with other R^{3+} cations (Hawthorne 1983). Changes in the content of Fe^{3+} on M1, M2, and M3 in amphibole may be obtained from measured mean bond-lengths in experimentally treated samples (Phillips et al. 1989). These authors, for example, showed that experimental oxidation-dehydrogenation of tschermakitic hornblende was accompanied by shortening of the mean bond-lengths ⟨M1-O⟩ and ⟨M3-O⟩ and lengthening of ⟨M2-O⟩, corresponding to increased Fe^{3+} on the M1 and M3 sites and decreased Fe^{3+} on M2. Gain or loss of Fe^{3+} on a site Mi resulting from experimental treatment may be estimated from changes in $\Delta\langle Mi\text{-}O\rangle$ as a function of change in Fe^{3+} pfu using the linear fits of Hawthorne (1983), where $\Delta\langle Mi\text{-}O\rangle = \langle Mi\text{-}O\rangle_{calc} - \langle Mi\text{-}O\rangle_{obs}$ and $\langle Mi\text{-}O\rangle_{calc}$ assumes that all Fe is Fe^{2+}. A positive slope for $\Delta\langle Mi\text{-}O\rangle$ vs. Fe^{3+} pfu shows that a small trivalent cation such as Fe^{3+} is increasing on that site with increasing oxidation (Phillips et al. 1989, Fig. 1). In our samples, heat treatment on the CCH_4 buffer (reduction-hydrogenation) resulted in increased values of $\Delta\langle Mi\text{-}O\rangle$ for M1 (0.001 to 0.005, average 0.003 Å) and M3 (−0.001 to 0.006, average 0.002 Å) and decreased values for M2 (−0.005 to 0.003 Å, average −0.0014 Å). Heating-induced changes in total Fe^{3+} and Fe^{2+} in our samples were small; the mean bond-length changes are not more than the precision of measurement (mostly 0.002 to 0.003 Å, Table 7), but at face value the changes are the reverse of those to be expected from the loss during heat treatment of Fe^{3+} on M1 and M3. We saw earlier that the Fe^{3+}/Fe^{2+} ratios inferred from ⟨M2-O⟩ are in approximate agreement with the photochemical data. Distortions of the M1-O and M3-O octahedra that could be related to hydrogenation, such as changes with heat treatment in the ratios (M1-O3)/⟨M1-O⟩ and (M3-O3)/⟨M3-O⟩, are small and inconsistent. Strictly speaking, our bond-length data are inconclusive regarding this issue; they neither prove nor disprove the presence of Fe^{3+} on M1 or M3 in our mildly dehydrogenated natural actinolites and ferroactinolites. Interestingly, Skogby and Annersten (1985) reported significantly increased Fe^{2+} on M2 in actinolite as a result of heat treatment in a hydrogen atmosphere at 600 °C. Possibly there is a difference in the crystal chemical response to dehydrogenation between the actinolites and the hornblendes that already have much $^{[6]}$Al on M2. Lacking evidence to the contrary, we will first examine $Fe^{2+}/(Fe^{2+} + Mg)$ ratios on sites under the assumption that all Fe^{3+} is located on M2, even though our samples are possibly up to 7% dehydrogenated (Table 4).

From the listing of M-site occupancies (Table 11) the projected ratios $Fe^{2+}/(Fe^{2+} + Mg)$ on sites ($= X_{Fe^{2+}}$) are plotted against each other in three Roozeboom diagrams (Fig. 4). All Fe on M1, M3, and M4 is assumed to be Fe^{2+}, and for the moment, Fe^{3+} based on the preferred values for Fe^{2+}/total Fe given in Table 2 is considered ordered on M2 (as in Table 11).

Figure 4b shows a small but consistent preference in the actinolite series for Fe^{2+} in favor of the M1 site over the M3 site; the mean intracrystalline partition coefficient K_D [$= (Fe/Mg)^{M1}/(Fe/Mg)^{M3}$] in all crystals is 1.22 ± 0.18. This establishes a point for non-aluminous calcic amphibole; K_D decreases with increasing occupancy of M2 by R^{3+} (Ungaretti et al. 1983). For cummingtonite-grunerite (Hirschmann et al. 1994) K_D is 1.09 ± 0.31, but both series, cummingtonite and actinolite, show no consistent detectable change in Fe-Mg site preference between unheated and heat-treated samples.

In unheated samples, Mg clearly prefers M2 over M1 (Fig. 4a), but heat treatment at 700 °C renders the partitioning close to equal: $K_D = 1.08 \pm 0.10$, where $K_D = (Fe^{2+}/Mg)^{M1}/(Fe^{2+}/Mg)^{M2}$. The same trend with an increase in equilibration temperature was observed in Mössbauer spectra by Skogby and Annersten (1985), Skogby (1987), and Skogby and Ferrow (1989) for tremolite and Mg-rich actinolite. The unheated crystals no doubt underwent variable cooling rates in nature and so cannot be expected to define a unique isotherm. The results for sample 11B at 600, 700, and 800 °C are identical, within the uncertainty limits (Table 11). In comparison to the actinolite series, both unheated and heat-treated crystals of cummingtonite-grunerite show stronger preference for Mg on M2 over M1 (Hirschmann et al. 1994), and this difference could be reflective of the relative different mean bond-lengths (⟨M2-O⟩ vs. ⟨M1-O⟩) in the two se-

TABLE 11. Occupancies of the M sites in actinolite

Sample no.	93728	C78	67-3172	C70	67-3701	C71	156831	C79	11B
Heat treatment (°C)	none	700	none	700	none	700	none	700	none
				M1					
Fe*	0.097(3)	0.108(4)	0.168(3)	0.185(2)	0.200(6)	0.217(3)	0.332(4)	0.381(5)	0.567(5)
Fe^{2+}	0.095	0.106	0.165	0.183	0.197	0.214	0.324	0.375	0.564
Mn	0.002	0.002	0.003	0.002	0.003	0.003	0.008	0.006	0.003
Mg	0.903	0.892	0.832	0.815	0.800	0.783	0.668	0.619	0.433
$Fe^{2+}/(Fe^{2+} + Mg)$	0.095	0.106	0.166	0.183	0.198	0.215	0.327	0.377	0.566
				M2					
Fe*	0.095(3)	0.099(4)	0.200(3)	0.222(2)	0.252(6)	0.266(3)	0.306(4)	0.401(5)	0.508(5)
Fe^{3+}	0.040	0.018	0.071	0.047	0.090	0.058	0.069	0.058	0.069
Fe^{2+}	0.052	0.076	0.123	0.170	0.156	0.201	0.220	0.328	0.431
Mn	0.003	0.005	0.006	0.005	0.006	0.007	0.017	0.015	0.008
Mg	0.873	0.856	0.773	0.764	0.722	0.723	0.653	0.534	0.490
Al	0.031	0.045	0.020	0.012	0.016	0.009	0.041	0.059	0.002
Ti	0.001	0.000	0.007	0.002	0.010	0.002	0.001	0.006	0.000
$Fe^{2+}/(Fe^{2+} + Mg)$	0.056	0.082	0.137	0.182	0.177	0.217	0.252	0.380	0.468
				M3					
Fe*	0.095(6)	0.092(6)	0.131(5)	0.133(4)	0.183(9)	0.178(5)	0.296(6)	0.344(8)	0.510(8)
Fe^{2+}	0.095	0.092	0.131	0.133	0.183	0.178	0.296	0.344	0.510
Mg	0.905	0.908	0.869	0.867	0.817	0.822	0.704	0.656	0.490
$Fe^{2+}/(Fe^{2+} + Mg)$	0.095	0.092	0.131	0.133	0.183	0.178	0.296	0.344	0.510
				M4					
Fe*	0.056	0.054	0.022	0.007	0.033	0.022	0.009	0.039	0.063
Fe^{2+}	0.053	0.051	0.021	0.007	0.032	0.021	0.008	0.037	0.062
Mn	0.003	0.003	0.001	0.000	0.001	0.001	0.001	0.002	0.001
Mg	0.011	0.013	0.002	0.003	0.009	0.007	0.009	0.001	0.000
Ca	0.901	0.887	0.952	0.977	0.928	0.945	0.961	0.949	0.919
Na	0.032	0.046	0.024	0.013	0.030	0.026	0.023	0.011	0.018
$Fe^{2+}/(Fe^{2+} + Mg)$	0.83	0.80	0.91	0.69	0.78	0.75	0.48	0.97	1.00

Note: All Fe^{3+} is assumed to be on M2.

ries. The two unheated samples of actinolite containing appreciable fluorine (67-3172 and 67-3701) are slightly discordant with the remainder; the substitution of F for OH on the O3 site can be expected to destabilize Fe^{2+} on M1 and M3 but not M2; or, alternatively, we have underestimated Fe^{3+} in these two samples.

The Roozeboom plot for M2 vs. M3 (Fig. 4c) resembles that for M2 vs. M1, but data points are displaced to smaller abscissa values. The result is that heat treatment has apparently reversed the Mg-Fe^{2+} site preference; the K_D for heated samples is 0.90 ± 0.12. This behavior was unexpected because models for intrasite partition have commonly assumed that configurational entropy is maximized as temperature is increased, although olivine is apparently an exception (Artioli et al. 1995). The behavior is accentuated in the two F-rich samples. Such a reversal in preference for M2 vs. M3 did not occur as a result of heat treatment of cummingtonite-grunerite. The extent of reversal is not great, and must be evaluated in the context of instrumental uncertainty of refined X_{Fe} on M3, which is greater than on M1 and M2 (Table 11), and the general problem of amount and location of Fe^{3+}. Heat-treated samples 11B and 12BA show excellent reproducibility in Figure 4c (where four data points overlap) and are consistent in Fe-Mg site preference with the more Fe-rich, also near-binary heated ferro-actinolite ID4-4C. For purposes of inter-laboratory comparison, two crystals A(1) and A(2) of heat-treated ID4-4C (C51) were also refined and unconstrained by Frank Hawthorne at the University of Manitoba with the following results for X_{Fe^*} [in the order crystals A(1), A(2), and C51 from Table 11]: M1 0.600(9), 0.619(9), 0.621(3); M2 0.617(8), 0.629(9), 0.643(3), M3 0.583(6), 0.596(6), 0.590(4), M4 0.028(6), 0.079(6), 0.072. In terms of relative site preferences, these data are in agreement within the limits of experimental error.

In Figure 5, Roozeboom plots were calculated by assuming that anion charge-balanced Fe^{3+} (related to dehydrogenation) is located on M1, and cation charge-balanced Fe^{3+} is located on M2 (this equivalent of Table 11 is available on request). In contrast to assuming that all Fe^{3+} is on M2, a reversal is suggested in Mg-Fe^{2+} partitioning for heat-treated samples (Fig. 5a) between M1 and M2 (K_D = 0.92 ± 0.06 at 700 °C) as well as between M3 and M2 (Fig. 5c). Fe^{2+} and Mg on M1 and M3 (Fig. 5b) are more nearly completely disordered than before (mean K_D = 1.09 ± 0.20 vs. 1.40 ± 0.25), and there remains no temperature dependency. Now, at 700 °C, the site preferences are: $X^{M2}_{Fe^{2+}} > X^{M1}_{Fe^{2+}} = X^{M3}_{Fe^{2+}}$. This exercise emphasizes the sensitivity of possible partition reversal in the actinolite series to the problems of Fe^{3+} analysis and the structural location of the minor amounts of Mn and Fe^{3+}. We are reluctant at this stage to conclude that the reversal behavior is real. At the very least, we can conclude overall that Fe^{2+}-Mg ordering on the octahedral sites is slight, and that for low-F actinolite Mg is enriched on M2 with slow cooling.

Additional light may perhaps be shed on the issue of

TABLE 11—*Continued*

C46 600	C28 700	C41 800	12BA none	C60 700	44973 none	C59 700	ID4-4C none	C51 700	168215 none	C80 700
					M1					
0.530(2)	0.538(3)	0.539(2)	0.559(4)	0.527(3)	0.602(3)	0.598(3)	0.643(3)	0.621(3)	0.867(5)	0.850(5)
0.527	0.534	0.536	0.553	0.522	0.557	0.557	0.631	0.610	0.841	0.827
0.003	0.004	0.003	0.006	0.005	0.045	0.041	0.012	0.011	0.026	0.023
0.470	0.462	0.461	0.441	0.473	0.398	0.402	0.357	0.379	0.133	0.150
0.529	0.536	0.538	0.557	0.524	0.583	0.581	0.639	0.617	0.863	0.846
					M2					
0.535(2)	0.544(3)	0.543(2)	0.500(4)	0.547(3)	0.581(3)	0.626(3)	0.584(3)	0.643(3)	0.823(5)	0.856(5)
0.054	0.055	0.055	0.094	0.053	0.155	0.084	0.062	0.063	0.060	0.062
0.472	0.479	0.479	0.394	0.479	0.330	0.432	0.494	0.549	0.694	0.730
0.009	0.010	0.009	0.012	0.015	0.096	0.110	0.028	0.031	0.069	0.064
0.465	0.456	0.455	0.499	0.452	0.392	0.335	0.409	0.357	0.176	0.142
0.000	0.000	0.002	0.000	0.000	0.025	0.037	0.006	0.000	0.000	0.000
0.000	0.000	0.000	0.001	0.000	0.002	0.003	0.001	0.000	0.001	0.002
0.504	0.512	0.513	0.441	0.514	0.457	0.564	0.547	0.606	0.798	0.837
					M3					
0.479(4)	0.483(4)	0.483(4)	0.515(7)	0.495(5)	0.555(5)	0.541(5)	0.592(4)	0.590(4)	0.772(8)	0.842(8)
0.479	0.483	0.483	0.515	0.495	0.555	0.541	0.592	0.590	0.772	0.842
0.521	0.517	0.517	0.485	0.505	0.445	0.459	0.408	0.410	0.228	0.158
0.479	0.483	0.483	0.515	0.495	0.555	0.541	0.592	0.590	0.772	0.842
					M4					
0.064	0.069	0.068	0.059	0.036	0.076	0.085	0.077	0.072	0.012	0.015
0.063	0.068	0.067	0.057	0.035	0.059	0.068	0.073	0.068	0.009	0.012
0.001	0.001	0.001	0.002	0.001	0.017	0.017	0.004	0.004	0.003	0.003
0.016	0.021	0.018	0.015	0.025	0.012	0.023	0.007	0.012	0.000	0.000
0.885	0.890	0.891	0.912	0.936	0.886	0.868	0.907	0.907	0.985	0.976
0.035	0.020	0.023	0.014	0.003	0.026	0.024	0.009	0.009	0.003	0.009
0.78	0.76	0.79	0.79	0.58	0.83	0.75	0.91	0.85	1.00	1.00

partition reversal by further consideration of bond valences. As shown earlier, the bond valence of O4 is strongly deficient. To satisfy the bond-valence requirements of O4, the bond lengths of T2-O4, M2-O4, and M4-O4 tend to be as short as possible. Because the T2 and M4 sites in the actinolite series are predominantly occupied by Si and Ca, respectively, the bond valences of T2 and M4 to O4 should not vary significantly with macroscopic X_{Fe}. Hence the contribution of bond valence from M2 becomes the most critical for the bond-valence requirement for O4. A strengthening of the M2-O4 bond may be achieved either by incorporating more higher-valence cations or by introducing more Fe^{2+} into the M2 site as Fe^{2+} can form the stronger covalent bond (considering the short M2-O4 bond distance, e.g., Ghose 1982). For a given composition, it is apparent that only the latter case is possible. Therefore, there appear to be two major, but competitive driving forces controlling the Fe-Mg ordering state of the M2 site at high temperature; one is to increase entropy (disorder) and the other is to reduce the bond-valence deficiency of O4 through increasing the Fe^{2+} content. Our data perhaps suggest that the latter driving force prevails in the actinolite series at high temperature at least up to 700 °C. For cummingtonite-grunerite, the bond-valence deficiency of O4 is not as large as that in the actinolites; thus, the former driving force dominates.

Because M4 is largely occupied by Ca, refined values of $X_{Fe^{2+}}$ [Fe/(Fe+Mg)] on M4 are not very accurate and are not figured. The refinements nevertheless suggest a small amount of Mg on M4 in most samples (Table 11), more than 1% in our most Mg-rich sample (as in tremolite, Yang and Evans 1996), and in some of the ferro-actinolites equilibrated at high temperature. $X_{Fe^{2+}}$ on M4 is larger than $X_{Fe^{2+}}$ on all other sites, as in cummingtonite-grunerite. In fact, heat treatment increased the refined X_{Mg} on M4, as also found by Skogby and Annersten (1985), Skogby (1987), and Skogby and Ferrow (1989) using Mössbauer spectroscopy.

Unit-cell dimensions

The lengths of unit-cell edges of the actinolite series all increase with macroscopic (Fe + Mn)/(Fe + Mn + Mn), the relative changes being: $a \geq b > c$ (Fig. 6), with the change in c less than half that in b. This behavior suggests similar mechanisms for chemical and thermal expansion (Sueno et al. 1973). On the other hand, under increased pressure, a of tremolite compresses twice as much as b and c (Comodi et al. 1991). As expected from a comparison with cummingtonite-grunerite (Hirschmann et al. 1994, Fig. 1), the a dimension is noticeably shorter for actinolites with more cummingtonite in solid solution. This is the case for the natural tremolite studied by Papike et al. (1969) and Sueno et al. (1973), and the synthetic ferro-actinolite of Ernst (1966), and indeed for many natural actinolites. The β angle increases, if at all, by no more than 0.1° from Mg to Fe end-member. On the other hand, the β angle correlates well with the content of Ca on M4, increasing from 104.55° in specimens with 10% cummingtonite solid solution to 104.80° in those with 1–

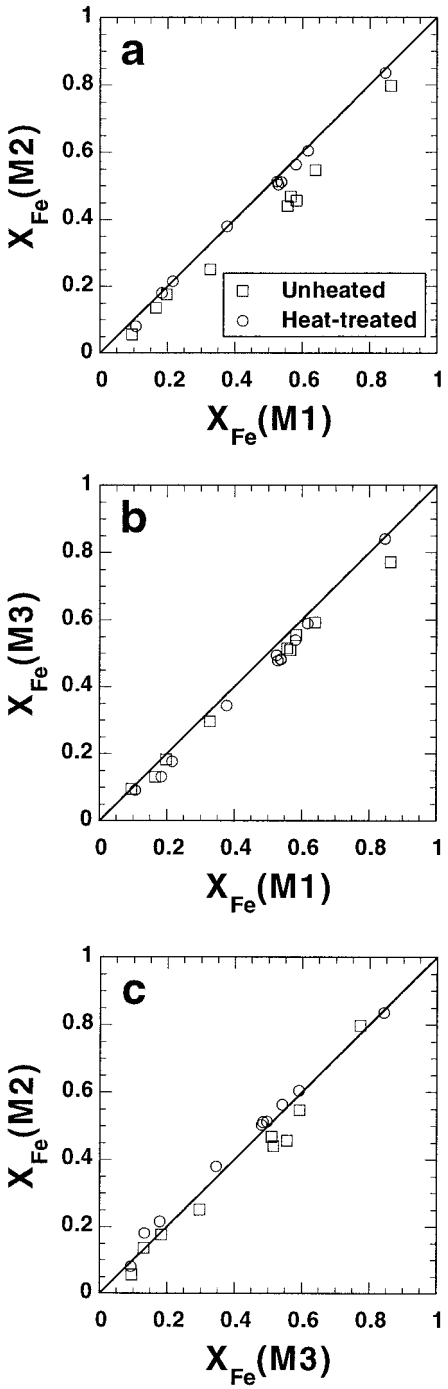

FIGURE 4. Roozeboom plots of M1, M2, and M3 site preferences in the actinolite series, assuming all Fe^{3+} is on M2. X_{Fe} = $Fe^{2+}/(Fe^{2+}$ + Mg) on sites. Open squares = untreated; open circles = heat treated (Table 2).

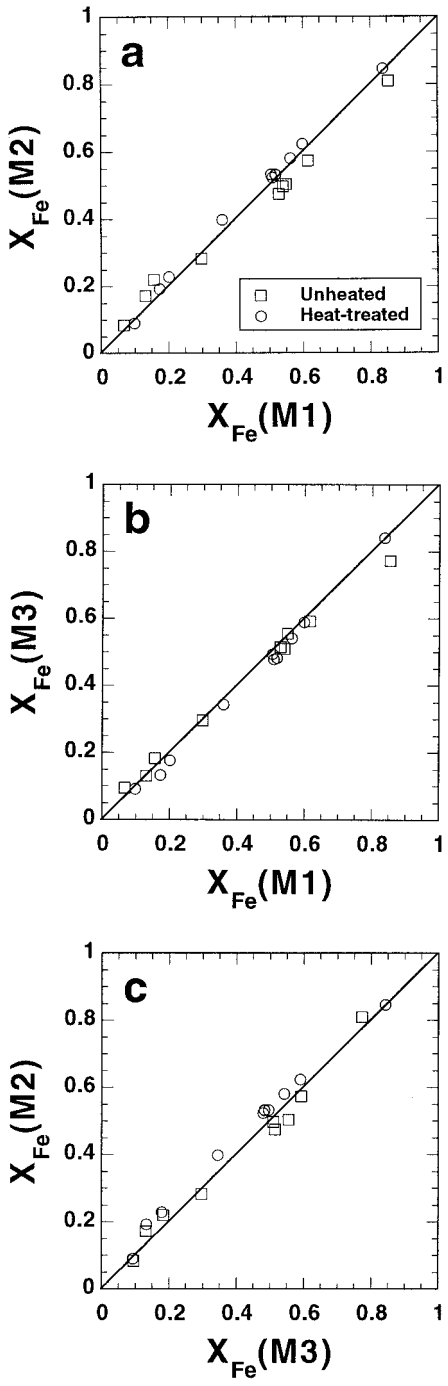

FIGURE 5. Roozeboom plots of M1, M2, and M3 site preference in the actinolite series, this work, assuming Fe^{3+} is located on M1 and M2 (see text).

2% of cummingtonite (Fig. 7). These variations are consistent with β of the end-members magnesio-cummingonite and grunerite being 101.9° and 102.1°, respectively (Hirschmann et al. 1994). With rare exceptions (Maresch et al. 1994), all synthetic tremolites and actinolites have β in the range 104.5° to 104.65°, and are therefore cummingtonite- or grunerite-bearing (Yang and Evans 1996). As expected from the small heat-induced changes in M-site ordering, no detectable systematic differences in cell dimensions between unheated and heated samples are apparent.

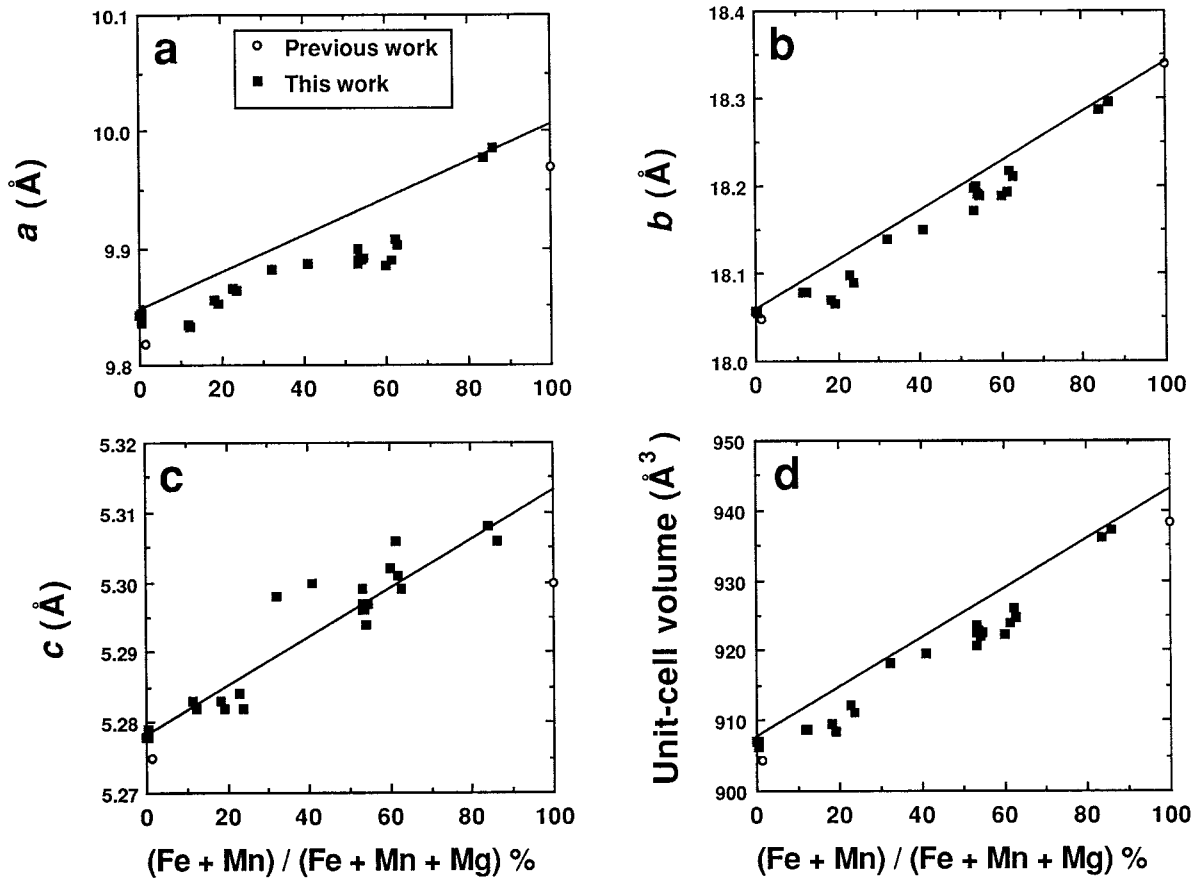

FIGURE 6. Cell dimensions as a function of macroscopic (Fe + Mn)/(Fe + Mn + Mg)%. Filled squares = actinolite and ferro-actinolite (this work) and tremolite (Yang and Evans 1996); circles = natural tremolite of Papike et al. (1969) and synthetic ferro-actinolite of Ernst (1966). Straight line connects inferred dimensions of end-members tremolite and ferro-actinolite (see text).

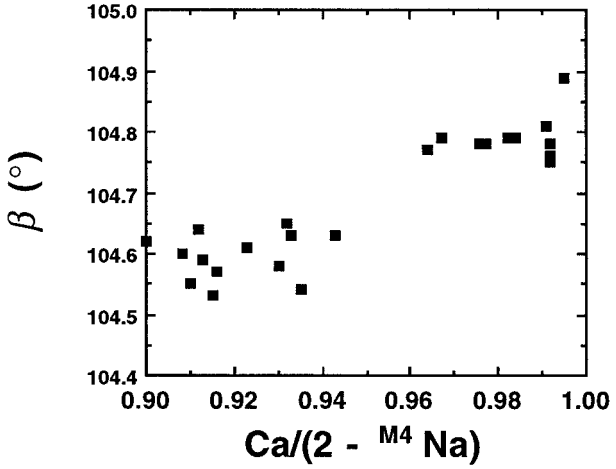

FIGURE 7. Variation of β of actinolite series with content of cummingtonite or grunerite solution, expressed in projection as Ca/(2 − ^{M4}Na) or mole fraction actinolite. Data from this work, Yang and Evans (1996) and Papike et al. (1969).

The volumes of natural samples of the actinolite series correlate imperfectly with (Fe + Mn)/(Fe + Mn + Mg)% owing to variable contents of cummingtonite solid solution, Al, and F, all of which tend to shrink the cell volume (Fig. 6d). A unit-cell volume of 907.0(2)Å^3 for end-member tremolite (Ca/Mg = 0.4) was established by Yang and Evans (1996), a value larger than almost all natural and synthetic tremolites owing to their tendency to contain some cummingtonite component in solid solution. A first approximation of the cell volume for end-member ferro-actinolite of 942.8 Å^3 may be derived by assuming a reciprocal (quadrilateral) ΔV of zero, that is: $V_{Fac} = V_{tr} + \frac{5}{7}(V_{gru} - V_{cum})$, where V_{Fac}, V_{tr}, V_{gru}, and V_{cum} are the volumes of end-members ferro-actinolite, tremolite, grunerite, and cummingtonite, respectively. A possible set of cell dimensions for end-member ferro-actinolite consistent with this volume and Figure 6 is: a = 10.01 Å, b = 18.34 Å, c = 5.313 Å, and β = 104.83°. This cell volume corresponds to a molar volume of ferro-actinolite of 2.8388 J/bar, somewhat larger than the volumes of 2.828 J/bar adopted by Holland and Powell (1990) and 2.8170 J/bar by Mäder and Berman (1992). Ferro-actinolite sample NMNH 168215 and its heated equivalent C80 are

very nearly binary in composition (with 0.3% cummingtonite, Al = 0.02, and Na + K = 0.04 pfu) and lie close to the straight line joining the volumes of the end-members (Fig. 6d).

Acknowledgments

For providing samples, we thank the National Museum of Natural History, Washington DC, the American Museum of Natural History, New York, The Natural History Museum, London, and R.G. Burns, R.F. Dymek, M.T. Einaudi, C. Klein, and L.D. Meinert. J.W. Stucki, J. Wu, and M.D. Dyar are thanked for Fe^{3+} estimates. S.M. Kuehner provided invaluable assistance with microprobe analysis. Constructive reviews were provided by R. Oberti, M. Welch, and F.C. Hawthorne, and we greatly appreciate the cooperation of Frank Hawthorne with inter-laboratory calibration of refinements. Discussions with many of the above, and with M.S. Ghiorso, R.M. Hazen, M.M. Hirschmann, C.T. Prewitt, and J.R. Smyth were most helpful. We are grateful for support from the National Science Foundation, through grants EAR-9303972 and EAR-9628203. H. Yang acknowledges support from a postdoctoral fellowship at the Carnegie Institution of Washington.

References cited

Ahn, J.H., Cho, M., Jenkins. D.M., and Buseck, P.R. (1991) Structural defects in synthetic tremolitic amphiboles. American Mineralogist, 76, 1811–1823.

Artioli, G., Rinaldi, R., Wilson, C.C., and Zanazzi, P.F. (1995) High-temperature Fe-Mg cation partitioning in olivine: In situ single-crystal neutron diffraction study. American Mineralogist, 80, 197–200.

Atkinson, W.W. and Einaudi, M.T. (1978) Skarn formation and mineralization in the contact aureole at Carr Fork, Bingham, Utah. Economic Geology, 73, 1326–1365.

Bocchio, R., Ungaretti, L., and Rossi, G. (1978) Crystal chemical study of eclogitic amphiboles from Alpe Arami, Lepontine Alps, southern Switzerland. Rendiconti della Società Italiana di Mineralogia e Petrologia, 34, 453–470.

Brown, I.D. (1981) The bond-valence method: An empirical approach to chemical structure and bonding. In M. O'Keefe and A. Navrotsky, Eds., Structure and Bonding in Crystals, 2, p. 1–30. Academic Press, New York.

Burns, R.G. and Greaves, C.J. (1971) Correlations of infrared and Mössbauer site population measurements of actinolites. American Mineralogist, 56, 2010–2033.

Clowe, C.A., Popp, R.K., and Fritz, S.J. (1988) Experimental investigation of the effect of oxygen fugacity on ferric-ferrous ratios and unit-cell parameters of four natural clinoamphiboles. American Mineralogist, 73, 487–499.

Comodi, P., Mellini, M., Ungaretti, L., and Zanazzi, P.F. (1991) Compressibility and high pressure structure refinement of tremolite, pargasite and glaucophane. European Journal of Mineralogy, 3, 485–499.

Dymek, R.F. and Klein, C. (1988) Chemistry, petrology and origin of banded iron-formation lithologies from the 3800 Ma Isua supracrustal belt, West Greenland. Precambrian Research 39, 247–302.

Ernst, W.G. (1966) Synthesis and stability relations of ferrotremolite. American Journal of Science, 264, 37–65.

Evans, B.W. and Ghiorso, M.S. (1995) Thermodynamics and petrology of cummingtonite. American Mineralogist, 80, 649–663.

Ghiorso, M.S., Evans, B.W., Hirschmann, M.M., and Yang, H. (1995) Thermodynamics of the amphiboles: Fe-Mg cummingtonite solid solutions. American Mineralogist, 80, 502–519.

Ghose, S. (1965) A scheme of cation distribution in the amphiboles. Mineralogical Magazine, 35, 46–54.

———(1982) Subsolidus reactions and microstructures in amphiboles. In Mineralogical Society of America Reviews in Mineralogy, 9A, 325–368.

Goldman, D.S. (1979) A reevaluation of the Mössbauer spectroscopy of calcic amphiboles. American Mineralogist, 64, 109–118.

Goldman, D.S. and Rossman, G.R. (1977) The identification of Fe^{2+} in the M(4) site of calcic amphiboles. American Mineralogist, 62, 205–216.

Hawthorne, F.C. (1978) The crystal chemistry of the amphiboles. VI. The stereochemistry of the octahedral strip. Canadian Mineralogist, 16, 37–52.

———(1983) The crystal chemistry of the amphiboles. Canadian Mineralogist, 21, 173–480.

Hawthorne, F.C. and Grundy, H.D. (1972) Positional disorder in the A-site of clino-amphiboles. Nature Physical Science, 235, 72–73.

———(1973) The crystal chemistry of the amphiboles. I. Refinement of the crystal structure of ferrotschermakite. Mineralogical Magazine, 39, 36–48.

———(1977) The crystal chemistry of the amphiboles. III. Refinement of the crystal structure of sub-silicic hastingsite. Mineralogical Magazine, 41, 43–50.

———(1978) The crystal chemistry of the amphiboles. VII. The crystal structure and site chemistry of potassium ferri-taramite. Canadian Mineralogist, 16, 53–62.

Hawthorne, F.C., Griep, J.L., and Curtis, L. (1980) A three-amphibole assemblage from the Tallan Lake sill, Peterborough County, Ontario. Canadian Mineralogist, 18, 275–284.

Hirschmann, M., Evans, B.W., and Yang, H. (1994) Composition and temperature dependence of Fe-Mg ordering in cummingtonite-grunerite as determined by X-ray diffraction. American Mineralogist, 79, 862–877.

Holland, T.J.B. and Powell, R. (1990) An enlarged and updated internally consistent thermodynamic dataset with uncertainties and correlations: The system K_2O-Na_2O-CaO-MgO-MnO-FeO-Fe_2O_3-Al_2O_3-TiO_2-SiO_2-C-H_2-O_2. Journal of Metamorphic Geology, 8, 89–124.

Kennedy, G.C. (1953) Geology and mineral deposits of Jumbo Basin, Southeast Alaska. United States Geological Survey, Professional Paper, 251, 46 p.

Klein, C. (1966) Mineralogy and petrology of the metamorphosed Wabash iron formation, Southwestern Labrador. Journal of Petrology, 7, 246–305.

Komadel, P. and Stucki, J.W. (1988) Quantitative assay of minerals for Fe^{2+} and Fe^{3+} using 1,10-phenanthrolene: III. A rapid photochemical method. Clays and Clay Minerals, 36, 379–381.

Leake, B.E. (1968) A catalog of analyzed calciferous and subcalciferous amphiboles together with their nomenclature and associated minerals. Geological Society of America Special Paper 98.

Litvin, A.L. (1973) Calcic amphiboles (structure, cation distribution, unit cell dimensions). Naukova Dumka, Kiev (in Russian).

Litvin, A.L., Egorova, L.N., Michnik, T.L., Ostapenko, S.S., and Tepikin, V.E. (1972) Structural refinements of actinolite and iron-rich hornblende. Mineralogicheskiy Sbornik, L′vov,26, 341–350 (in Russian).

Mäder, U.K. and Berman, R.G. (1992) Amphibole thermobarometry: A thermodynamic approach, In Current Research, Part E. Geological Survey of Canada, Paper 92-1E, 1–8.

Makino, K. and Tomita, K. (1989) Cation distribution in the octahedral sites of hornblendes. American Mineralogist, 74, 1097–1105.

Maresch, W.V., Czank, M., and Schreyer, W. (1994) Growth mechanisms, structural defects and composition of synthetic tremolite: What are the effects on macroscopic properties? Contributions to Mineralogy and Petrology, 118, 297–313.

McGavin, D.G., Palmer, R.A., Tennant, W.C., and Devine, S.D. (1982) Use of ultrasonically modulated electron resonance to study S-state ions in mineral crystals: Mn^{2+}, Fe^{3+} in tremolite. Physics and Chemistry of Minerals, 8, 200–205.

Mitchell, J.T., Bloss, F.D., and Gibbs, G.V. (1970) A refinement of the structure of actinolite. American Mineralogist, 55, 302–303.

———(1971) Examination of the actinolite structure and four other C2/m amphiboles in terms of double bonding. Zeitschrift für Kristallographie, 133, 273–300.

Mueller, R.F. (1960) Compositional characteristics and equilibrium relations in mineral assemblages of a metamorphosed iron formation. American Journal of Science, 258, 449–497.

Mustard, J.F. (1992) Chemical analysis of actinolite from reflectance spectra. American Mineralogist, 77, 345–358.

North, A.C.T., Phillips, D.C., and Mathews, F.S. (1968) A semi-empirical method of absorption correction. Acta Crystallographica, A24, 351–359.

Oberti, R., Ungaretti, L., Cannillo, E., and Hawthorne, F.C. (1993a) The

mechanism of Cl incorporation in amphibole. American Mineralogist, 78, 746–752.

Oberti, R., Hawthorne, F.C., Ungaretti, L., and Cannillo, E. (1993b) The behaviour of Mn in amphibole: Mn in richterite. European Journal of Mineralogy, 5, 43–51.

———(1995a). $^{[6]}$Al disorder in amphiboles from mantle peridotites. Canadian Mineralogist, 33, 867–878.

Oberti, R., Hawthorne, F.C., Ungaretti, L., Cannillo, E., and Memmi, I. (1995b) Temperature-dependent Al order-disorder in the tetrahedral double-chain of *C*2/*m* amphiboles. European Journal of Mineralogy, 7, 1049–1063.

Papike, J.J., Ross, M., and Clark, J.R. (1969) Crystal chemical characterization of clinoamphiboles based on five new structure refinements. Mineralogical Society of America Special Paper, 2, 117–136.

Phillips, M.W., Popp, R.K., and Clowe, C.A. (1988) Structural adjustments accompanying oxidation-dehydrogenation in amphiboles. American Mineralogist, 73, 500–506.

Phillips, M.W., Draheim, J.E., Popp, R.K., Clowe, C.A., and Pinkerton, A.A. (1989) Effects of oxidation-dehydrogenation in tschermakitic hornblende. American Mineralogist, 74, 764–773.

Popp, R.K., Virgo, D., Yoder, H.S., Hoering, T.C., and Phillips, M.W. (1995) An experimental study of phase equilibria and Fe oxy-component in kaersutitic amphibole: Implications for the f_{H_2} and a_{H_2O} in the upper mantle. American Mineralogist, 80, 534–548.

Robinson, K., Gibbs, G.V., and Ribbe, P.H. (1971) Quadratic elongation: A quantitative measure of distortion in coordination polyhedra. Science, 172, 567–570.

Robinson, K., Gibbs, G.V., Ribbe, P.H., and Hall, M.R. (1973) Cation distribution in three hornblendes. American Journal of Science, 273A, 522–535.

Shannon, R.D. (1976) Revised effective ionic radii and systematic studies of interatomic distances in halides and chalcogenides. Acta Crystallographica, A32, 751–767.

Shannon, R.D. and Prewitt, C.T. (1969) Effective ionic radii for oxides and halides. Acta Crystallographica, B25, 925–946.

Skogby, H. (1987) Kinetics of intracrystalline order-disorder reactions in tremolite. Physics and Chemistry of Minerals, 14, 521–526.

Skogby, H. and Annersten, H. (1985) Temperature dependent MgFe-cation distribution in actinolite-tremolite. Neues Jahrbuch für Mineralogie Monatshefte, 193–203.

Skogby, H. and Ferrow, E. (1989) Iron distribution and structural order in synthetic calcic amphiboles studied by Mössbauer spectroscopy and HRTEM. American Mineralogist, 74, 360–366.

Stucki, J.W. (1981) The quantitative assay of minerals for Fe^{2+} and Fe^{3+} using 1,10-phenanthrolene: II. A photochemical method. Soil Science Society of America Journal, 45, 638–641.

Stucki, J.W. and Anderson, W.L. (1981) The quantitative assay of minerals for Fe^{2+} and Fe^{3+} using 1,10-phenanthroline: I. Sources of variability. Soil Science Society of America Journal, 45, 633–637.

Sueno, S., Cameron, M., Papike, J.J., and Prewitt, C.T. (1973) The high temperature crystal chemistry of tremolite. American Mineralogist, 58, 649–664.

Ungaretti, L., Lombardo, L., Domeneghetti, C., and Rossi, G. (1983) Crystal chemical evolution of amphiboles from eclogitized rocks of the Sesia Lanzo Zone, Italian Alps. Bulletin de Mineralogie, 106, 645–672.

Wilkins, R.W.T. (1970) Iron-magnesium distribution in the tremolite-actinolite series. American Mineralogist, 55, 1993–1998.

Yang, H. and Hirschmann, M.M. (1995) Crystal structure of $P2_1/m$ ferromagnesian amphibole and the role of cation ordering and composition in the $P2_1/m$-$C2/m$ transition in cummingtonite. American Mineralogist, 80, 916–922.

Yang, H. and Evans, B.W. (1996) X-ray structure refinements of tremolite at 140 and 295 K: Crystal chemistry and petrologic implications. American Mineralogist, 81, 1117–1125.

Zanetti, A., Oberti, R., Bottazzi, P., and Vannucci, R. (1997) Fe^{3+} contents in partially dehydrogenated high-T amphiboles by combining SREF, EMP and SIMS analyses: An insight into intensive parameters of upper-mantle sytsems (abstract). Terra Nova Volume 9, Abstract Supplement No. 1, p. 437.

Manuscript received April 14, 1997
Manuscript accepted December 17, 1997
Paper handled by Nancy Ross